Recovering multiscale buried anomalies in a two-layered medium

2015 Inverse Problems 31 105006

(http://iopscience.iop.org/0266-5611/31/10/105006)

IOP Publishing Inverse Problems
Inverse Problems 31 (2015) 105006 (28pp) doi:10.1088/0266-5611/31/10/105006

Recovering multiscale buried anomalies in a two-layered medium

Jingzhi Li[1], Peijun Li[2], Hongyu Liu[3,5] and Xiaodong Liu[4]

[1] Faculty of Science, South University of Science and Technology of China, 518055 Shenzhen, People's Republic of China
[2] Department of Mathematics, Purdue University, West Lafayette, IN 47907, USA
[3] Department of Mathematics, Hong Kong Baptist University, Kowloon, Hong Kong SAR
[4] Institute of Applied Mathematics, Academy of Mathematics and Systems Science, Chinese Academy of Sciences, 100190 Beijing, People's Republic of China

E-mail: li.jz@sustc.edu.cn, lipeijun@math.purdue.edu, hongyu.liuip@gmail.com and xdliu@amt.ac.cn

Received 2 October 2014, revised 9 July 2015
Accepted for publication 4 August 2015
Published 15 September 2015

Abstract

We develop an inverse scattering scheme of recovering impenetrable anomalies buried in a two-layered medium. The recovery scheme works in a rather general setting and possesses several salient features. It makes use of a single far-field measurement in the half-space above the anomalies, and works independently of the physical properties of the anomalies. There might be anomalous components of multiscale sizes presented simultaneously. Moreover, the proposed scheme is of a totally direct nature without any inversion involved, and hence it is very fast and robust against measurement noise. Both theoretical foundation and numerical experiments are presented. This extends related results in the literature on recovering multiscale scatterers located in a homogeneous space.

Keywords: inverse scattering, buried anomalies, recovery scheme, single measurement, multiscale

1. Introduction

1.1. Motivation and background

In this work, we consider the recovery of anomalies buried in a two-layered medium; see figure 1 for a schematic illustration. Suppose the space is delimited by a flat plane Γ_0 into two

[5] Author to whom any correspondence should be addressed.

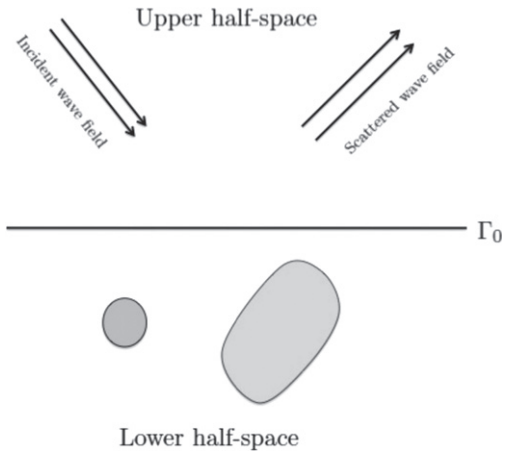

Figure 1. Schematic illustration of the anomalies detection in a two-layered medium.

half-spaces: the upper one and the lower one. The two half-spaces are occupied by two different (homogeneous) mediums. It is further supposed that some inhomogeneous anomalies are buried or immersed in the lower half-space. We are interested in recovering the anomalies by wave detection made in the upper half-space, which is proceeded as follows. One sends a certain wave field from the upper half-space, and then measures the perturbed wave field caused by the anomalies together with the ambient lower-space medium. The detecting wave field is referred to as the incident wave field and the perturbed wave field is referred to as the scattered wave field. The inverse problem that we are concerned with is to recover the anomalies by knowledge of the scattered wave field. Practical scenarios of our current study include the underground mineral prospection, mines locating in the battlefield, and anti-submarine detection.

The inverse scattering problem described above can be abstractly formulated as an operator equation,

$$F(\mathrm{O}) = \mathcal{M}, \tag{1.1}$$

where O denotes the anomalous object, and $\mathcal{M}$ denotes the wave measurement data. F is an operator which sends the anomaly to the corresponding measurement, defined by the forward wave scattering system. As a typical feature for various inverse scattering problems, (1.1) is nonlinear by noting that generally one has $F(\mathrm{O}_1 \cup \mathrm{O}_1) \neq F(\mathrm{O}_1) + F(\mathrm{O}_2)$, where O_1 and O_2 are two different anomalies. This is mainly due to the multiple wave scattering interaction between O_1 and O_2. Moreover, it is easily seen that the inverse problem (1.1) is ill-posed in the sense of Hadamard.

In order to tackle the nonlinearity of various inverse problems, a salient technique that has been widely investigated in the literature is the so-called sampling. A variety of schemes have been developed in this category, including the linear sampling method [8–10], the factorization method [15–17] and the MUSIC-type methods [1–3, 8, 13, 15] and a variety of methods using multifrequency data [5–7], among others. The cores of these methods are certain imaging functionals, which are used to indicate a space point belonging to the interior or the exterior of the scattering anomaly. The process of calculating those imaging functionals is linear and hence the nonlinearity of the inverse problem is reduced to the determination of the belongingness of any given space point, that can be easily visualized. In order to tackle the ill-posedness, various regularizations are incorporated into those schemes. Recently, a novel

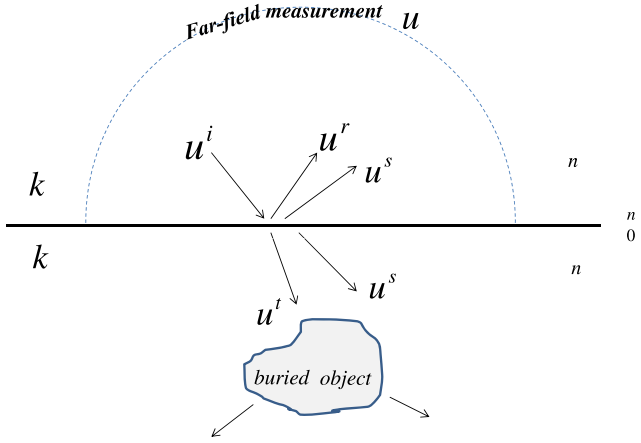

Figure 2. 2D scattering from buried anomalies in a two-layered medium.

sampling scheme was proposed for the inverse scattering problem of locating inhomogeneities embedded in a homogeneous space in [19–21]. The approach also relies on certain properly designed imaging functionals, whose calculations are totally direct without any inversion involved. More notably, the method makes use of only a single far-field measurement, which is much fewer than the existing methods in the literature. Hence, the method is very efficient and robust against measurement noise, and easy to implement as well. In this work, we extend the method to the practical and interesting case of recovering the multiscale anomalies buried in a two-layered medium as described earlier. The major novelty and difficulty of the current study are the inhomogeneous two-layered background medium.

Following a similar spirit to the study in [19–21], we develop the new recovery scheme in three steps. First, we consider the recovery of anomalies with small size compared to the detecting wavelength. This is based on linearizing the inverse problem (1.1). To that end, we derive the asymptotic expansion of scattered wave field in terms of the small diameter parameter of the underlying anomalies. Second, we consider the recovery of multiple regular-size anomalies. In this case, we require that the anomalies are from an admissible class, which is known in advance. The recovery is based on projecting the measured far-field pattern into a space of far-field patterns generated by the admissible scatterers. Finally, by concatenating the above two procedures via a local tuning technique, one can recover multiple multiscale buried anomalies. We would like to mention in passing that similar inverse problems of recovering buried objects were also considered in [4, 12] with different methods.

1.2. Mathematical formulation

For $x = (x^1, x^2, \cdots, x^n) \in \mathbb{R}^n$, $(n = 2, 3)$, we let

$$\mathbb{R}^n_+ := \{x \in \mathbb{R}^n : x^n > 0\} \quad \text{and} \quad \mathbb{R}^n_- := \{x \in \mathbb{R}^n : x^n < 0\},$$

be, respectively, the upper and lower half-spaces. The interface between the two layers, namely $\{x \in \mathbb{R}^n; x^n = 0\}$, is denoted by $\mathbb{R}^n_0$. Let k_+ and k_- be the wavenumbers in $\mathbb{R}^n_+$ and $\mathbb{R}^n_-$, respectively. Denote by Ω an impenetrable obstacle that is completely buried in the lower half-space (see figure 2). It is assumed that Ω is a bounded Lipschitz domain with connected

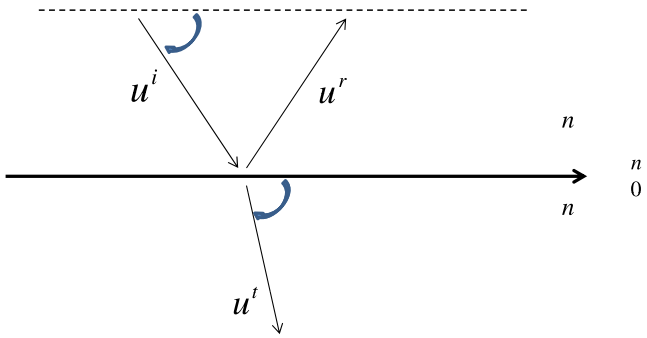

Figure 3. Incident plane wave u^i, reflected wave u^r and transmitted wave u^t.

complement. In what follows, we let ν denote the unit outward normal vector to $\partial\Omega$, as well as the unit upward normal vector to $\mathbb{R}^n_0$, which should be clear from the context.

Let u^i be a time-harmonic incident plane wave given by

$$u^i(x) = e^{ik_+ x\cdot d^i},$$

where $d^i \in \mathbb{S}^{n-1} := \{x \in \mathbb{R}^n;\ |x| = 1\}$ denotes the incident direction. In what follows, we set $\mathbb{S}^{n-1}_\pm := \mathbb{S}^{n-1} \cap \mathbb{R}^n_\pm$ and, let (r, θ) and (r, θ, φ) denote the standard polar coordinates in $\mathbb{R}^2$ and $\mathbb{R}^3$, respectively. Denote by $\theta_c \in (-\pi, 0]$ the critical incident angle which is defined by $\cos\theta_c = k_-/k_+$ if $k_- < k_+$ and $\theta_c = 0$ if $k_- \geqslant k_+$. We take the incident direction

$$d^i := \begin{cases} \big(\cos\theta_0\cos\varphi_0,\ \cos\theta_0\sin\varphi_0,\ \sin\theta_0\big), & n = 3; \\ \big(\cos\theta_0,\ \sin\theta_0\big), & n = 2, \end{cases} \tag{1.2}$$

where $\theta_0 \in (-\pi - \theta_c, \theta_c)$ is such that $d^i \in \mathbb{S}^{n-1}_-$, and $\varphi_0 \in (0, 2\pi)$. The interface $\mathbb{R}^n_0$ generates the reflected and transmitted wave fields, which shall be denoted as u^r and u^t, respectively. By the Fresnel formula, we have

$$u^r(x) = R\big(\theta_0\big)e^{ik_+ x\cdot d^r},\ x \in \mathbb{R}^n_+; \quad u^t(x) = T\big(\theta_0\big)e^{ik_- x\cdot d^t},\ x \in \mathbb{R}^n_-, \tag{1.3}$$

where d^r is the reflected direction and d^t is the transmitted direction (see figure 3 for an illustrative example), while $R(\theta_0)$ and $T(\theta_0)$ are the reflection and transmission coefficients, respectively. The corresponding reflected direction is given by

$$d^r = \begin{cases} \big(\cos\theta_0\cos\varphi_0,\ \cos\theta_0\sin\varphi_0,\ -\sin\theta_0\big), & n = 3; \\ \big(\cos\theta_0,\ -\sin\theta_0\big), & n = 2, \end{cases} \tag{1.4}$$

and the transmitted direction is given by

$$d^t = \begin{cases} \big(\cos\chi_0\cos\varphi_0,\ \cos\chi_0\sin\varphi_0,\ \sin\chi_0\big), & n = 3; \\ \big(\cos\chi_0,\ \sin\chi_0\big), & n = 2. \end{cases} \tag{1.5}$$

In (1.5), $\chi_0 \in (-\pi, 0)$ stands for the transmitted angle into $\mathbb{R}^n_-$, and is implicitly given by the Snell relation

$$k_+\cos\theta_0 = k_-\cos\chi_0. \tag{1.6}$$

Set

$$u_0(x) = \begin{cases} u^i(x) + u^r(x), & x^n > 0; \\ u^t(x), & x^n < 0. \end{cases}$$

It is required that both u_0 and $\partial u_0/\partial \nu$ are continuous across the interface $\mathbb{R}_0$. That is, $u^i + u^r - u^t = 0$ and $\partial(u^i + u^r)/\partial\nu - \partial(u^t)/\partial\nu = 0$ on $\mathbb{R}_0^n$. By using such continuities, one can deduce that the coefficients $R(\theta_0)$ and $T(\theta_0)$ are given according to the following formulas:

$$R(\theta) = \frac{k_+ \sin\theta - k_- \sin\chi}{k_+ \sin\theta + k_- \sin\chi} \quad \text{and} \quad T(\theta) = \frac{2k_+ \sin\theta}{k_+ \sin\theta + k_- \sin\chi}. \tag{1.7}$$

In particular, we note that if $k_+ = k_-$, then $R(\theta_0) = 0$, $T(\theta_0) = 1$ and $u_0 = u^i$.

With above preparations, the forward problem of the scattering due to the buried impenetrable anomalies in a two-layered medium can be described as finding the scattered wave field $u^s \in H^1_{loc}(\mathbb{R}^n \backslash \overline{\Omega})$ such that

$$\begin{aligned} \Delta u^s + (k_\pm)^2 u^s &= 0 \quad \text{in } \mathbb{R}^n_\pm \backslash \overline{\Omega}, \\ [u^s] = 0, \left[\frac{\partial u^s}{\partial \nu}\right] &= 0 \text{ on } \mathbb{R}_0, \\ \mathcal{B}(u^s) &= -\mathcal{B}(u_0) \quad \text{on } \partial\Omega, \\ \lim_{r\to\infty} \int_{\mathbb{S}_{r,\pm}} \left| \frac{\partial u^s}{\partial r} - ik_\pm u^s \right|^2 ds &= 0, \end{aligned} \tag{1.8}$$

where $[\,\cdot\,]$ denotes the jump in its argument across the interface $\mathbb{R}_0^n$, $\mathbb{S}_{r,\pm} = \{x \in \mathbb{R}^n_\pm; |x| = r\}$ is the half sphere/circle of radius r centered at the origin in $\mathbb{R}^n_\pm$ and $\mathcal{B}$ denotes one of the following three boundary conditions:

$$\mathcal{B}(u^s) = u^s \text{ on } \partial\Omega; \quad \mathcal{B}(u^s) = \frac{\partial u^s}{\partial \nu} \text{ on } \partial\Omega; \quad \mathcal{B}(u^s) = \frac{\partial u^s}{\partial \nu} + i\lambda u^s \text{ on } \partial\Omega \tag{1.9}$$

corresponding, respectively, to the case when the anomaly Ω is sound-soft, sound-hard, and of impedance type. In (1.9), $\lambda \in C(\partial\Omega)$, $(\lambda \geqslant 0)$, is the surface impedance. By a variational approach and following essentially a similar argument as in [11] or [24 section 12.4], one can establish the well-posedness of the scattering problem (1.2)–(1.9). For $x \in \mathbb{R}^n_+$, $u^s(x)$ admits the following asymptotic expansion

$$u^s(x) = \gamma_n \frac{e^{ik_+ r}}{r^{\frac{n-1}{2}}} \left\{ u^\infty(\hat{x}) + \mathcal{O}\left(\frac{1}{r}\right) \right\} \text{ as } r = |x| \to \infty \tag{1.10}$$

with

$$\gamma_n = \frac{1}{4\pi}, \ n = 3; \quad \frac{e^{i\frac{\pi}{4}}}{\sqrt{8k_+\pi}}, \ n = 2,$$

uniformly for all directions $\hat{x} := x/|x|$. In (1.10), $u^\infty(\hat{x})$ defined on the upper half unit sphere/circle $\mathbb{S}^{n-1}_+$ is known as the scattering amplitude or far-field pattern with $\hat{x} \in \mathbb{S}^{n-1}_+$ denoting the observation direction.

The inverse scattering problem that we are concerned with is to recover Ω by knowledge of $u_\infty(\hat{x})$. In terms of the abstract operator equation (1.1), Ω is the unknown O, u_∞ is the measurement data set $\mathcal{M}$, and F is defined by the direct scattering system as described in (1.2)–(1.10). Throughout the current study, we shall take d^i fixed. That is, the measurement

$u^\infty(\hat{x})$ is obtained by sending a single incident plane wave, and we call it a single far-field measurement.

2. Results on direct scattering problem

2.1. Green's function and its asymptotic behavior at infinity

For the subsequent use, we briefly present the Green function $G(x, y)$ of the two-layered scattering problem, i.e., the fundamental solution of the unperturbed problem (1.2)–(1.8) with $\Omega = \varnothing$, and discuss its asymptotic behavior at infinity.

For an observation point $x = (x^1, x^2, \cdots, x^n) \in \mathbb{R}^n_+$ and a source point $y = (y^1, \cdots, y^n) \in \mathbb{R}^n_-$, define $x' := (x^1, x^2, \cdots, x^{n-1})$ and $y' := (y^1, y^2, \cdots, y^{n-1})$. Let $\xi = (\xi^1, \cdots, \xi^{n-1}) \in \mathbb{R}^{n-1}$. Define $\eta_\pm := \sqrt{k_\pm^2 - |\xi|^2}$ with $\Im(\eta_\pm) \geqslant 0$. By using the transmission conditions across $\mathbb{R}^n_0$ and the Fourier transformation technique, one can derive that the Green function for $y^n < 0$ is given by (see e.g., [4])

$$G(x, y) = \begin{cases} G^t(x, y), & x \in \mathbb{R}^n_+; \\ G^i(x, y) + G^r(x, y), & x \in \mathbb{R}^n_-, x \neq y \end{cases} \tag{2.1}$$

with

$$G^i(x, y) := \begin{cases} \frac{e^{ik_-|x-y|}}{4\pi\,|\,x-y\,|}, & n = 3; \\ \frac{i}{4}H_0^{(1)}\big(k_-|x-y|\big), & n = 2, \end{cases} \tag{2.2}$$

$$G^t(x, y) := \frac{i}{2\pi}\int_{\mathbb{R}^{n-1}} \frac{e^{i\left(\eta_+ x^n - \eta_- y^n\right)}}{\eta_+ + \eta_-} e^{i\xi\cdot(x'-y')}d\xi \tag{2.3}$$

and

$$G^r(x, y) := \frac{i}{4\pi}\int_{\mathbb{R}^{n-1}} \frac{\eta_- - \eta_+}{\eta_-\left(\eta_+ + \eta_-\right)} e^{-i\eta_-(x^n+y^n)} e^{i\xi\cdot\left(x'-y'\right)}d\xi, \tag{2.4}$$

where $H_0^{(1)}$ is the Hankel function of the first kind and order zero.

Denote by $\hat{\theta}_c \in [0, \pi)$ the critical observation angle which is defined by $\cos\hat{\theta}_c = k_-/k_+$ if $k_- < k_+$ and $\hat{\theta}_c = 0$ if $k_- \geqslant k_+$. Since the observation for the inverse problem shall be made in the upper half-space $\mathbb{R}^n_+$, we are mainly interested in the asymptotic formula of $G^t(x, y)$, which is given by (cf [4])

$$G^t(x, y) = \gamma_n \frac{e^{ik_+ r}}{r^{\frac{n-1}{2}}}\left\{T\left(\theta_{\hat{x}}\right)e^{-ik_-\hat{x}^t\cdot y} + O\left(\frac{1}{r}\right)\right\}, \quad x = r\hat{x} \tag{2.5}$$

with

$$\hat{x} := \begin{cases} \left(\cos\theta_{\hat{x}}\cos\phi_{\hat{x}},\ \cos\theta_{\hat{x}}\sin\phi_{\hat{x}},\ \sin\theta_{\hat{x}}\right), & n = 3; \\ \left(\cos\theta_{\hat{x}},\ \sin\theta_{\hat{x}}\right), & n = 2, \end{cases} \tag{2.6}$$

where $\theta_{\hat{x}} \in (\hat{\theta}_c, \pi - \hat{\theta}_c)$, $\phi_{\hat{x}} \in (0, 2\pi)$ and

$$\hat{x}^t := \begin{cases} (\cos\chi_{\hat{x}} \cos\phi_{\hat{x}}, \ \cos\chi_{\hat{x}} \sin\phi_{\hat{x}}, \ \sin\chi_{\hat{x}}), & n = 3; \\ (\cos\chi_{\hat{x}}, \sin\chi_{\hat{x}}), & n = 2, \end{cases} \tag{2.7}$$

with $\chi_{\hat{x}} \in (0, \pi)$ uniquely determined by the relation

$$k_+ \cos\theta_{\hat{x}} = k_- \cos\chi_{\hat{x}}. \tag{2.8}$$

2.2. Translation relation

We first fix some notations that shall be used throughout the rest of the paper. Let D be a bounded simply connected Lipschitz domain in $\mathbb{R}^n_-$. For any $z \in \mathbb{R}^n_-$ and $\rho \in \mathbb{R}_+$, we define $z + D := \{z + x; x \in D\}$ and $\rho D := \{\rho x; x \in D\}$. Moreover, for a unitary rotation matrix $U \in SO(n)$, we define $UD := \{Ux; x \in D\}$. Let $\Omega = z + \rho UD$. We shall write the quaternion $(D; z, \rho, U)$ to represent the scatterer Ω. D is referred to as a *base*, and z, ρ and U are respectively referred to as the *location, size* and *orientation* of the scatterer Ω with respect to the base scatterer D. Throughout, we assume that $\Omega \subset \mathbb{R}^n_-$. Furthermore, it is assumed that the physical property of the scatterer Ω is inherited from the base scatterer D. That is, if D is sound-soft (resp. sound-hard or of impedance type), then Ω is also sound-soft (resp. sound-hard or of impedance type). We shall write D^s, D^h and D^i to indicate that the scatterer is sound-soft, sound-hard and of impedance type, respectively. In the case that D is of impedance type with the surface impedance parameter $\lambda(x)$ for $x \in \partial D$, then the surface impedance parameter for $\Omega = (D; z, \rho, U)$ is given by $\lambda(\frac{1}{\rho}U^T(x - z))$. Without the superscript indication, D could be a scatter of any of the three types.

In this section, we consider the scattering due to a translated obstacle $\Omega = (D; z) := (D; z, 1, I)$. In the sequel, we shall write the scattered wave as $u^s(\,\cdot\,; \Omega)$ in order to indicate its dependence on the underlying scatterer Ω. We need make use of the following Green formula,

$$u^s(x; \Omega) = \int_{\partial\Omega} \left\{ u^s(y; \Omega) \frac{\partial G(x, y)}{\partial \nu(y)} - G(x, y) \frac{\partial u^s(y; \Omega)}{\partial \nu(y)} \right\} ds(y), \quad x \in \mathbb{R}^n \backslash \overline{\mathbb{R}^n_0 \cup \Omega}, \tag{2.9}$$

whose proof follows from a similar argument to that of theorem 2.5 in [10]. Applying the asymptotic formula (2.5) of $G^t(x, y)$ to the Green formula (2.9), one can show by straightforward calculations that the scattering amplitude of $u^s(\,\cdot\,; \Omega)$ on $\mathbb{S}^{n-1}_+$ is given by

$$u^\infty(\hat{x}; \Omega) = T(\theta_{\hat{x}}) \int_{\partial\Omega} \left\{ u^s(y; \Omega) \frac{\partial e^{-ik_- \hat{x}^t \cdot y}}{\partial \nu(y)} - e^{-ik_- \hat{x}^t \cdot y} \frac{\partial u^s(y; \Omega)}{\partial \nu(y)} \right\} ds(y), \ \hat{x} \in \mathbb{S}^{n-1}_+. \tag{2.10}$$

Next, we present a relation of the scattering amplitude due to the translation of the underlying scatterer.

Lemma 2.1. *Let $\Omega = (D; z) \subset \mathbb{R}^n_-$. Then we have*

$$u^\infty(\hat{x}; \Omega) = e^{ik_-(d^t - \hat{x}^t)\cdot z} u^\infty(\hat{x}; D), \tag{2.11}$$

where d^t, $\hat{x}$ and $\hat{x}^t$ are given by (1.5), (2.6) and (2.7), respectively, satisfying the relations (1.6) and (2.8).

Proof. Since $e^{ik\_d^t\cdot z}$ is a constant, the boundary condition (1.9) implies that, for $y \in \partial\Omega$,

$$\mathcal{B}u^s(y;\,\Omega) = -\mathcal{B}u^t(y;\,\Omega) = -e^{ik\_d^t\cdot z}\mathcal{B}u^t(x;\,D) = e^{ik\_d^t\cdot z}\mathcal{B}u^s(x;\,D),$$

where $x = y - z \in \partial D$. By the uniqueness of the direct scattering problem one has

$$u^s(y;\,\Omega) = e^{ik\_d^t\cdot z}u^s(x;\,D), \quad \forall\, y \in \mathbb{R}^n\backslash\overline{\Omega}.$$

Therefore, we have for $y \in \partial\Omega$

$$u^s(y;\,\Omega) = e^{ik\_d^t\cdot z}u^s(x;\,D) \quad \text{and} \quad \frac{\partial u^s(y;\,\Omega)}{\partial\nu(y)} = e^{ik\_d^t\cdot z}\frac{\partial u^s(x;\,D)}{\partial\nu(x)},$$

which implies that

$$\begin{aligned}
&u^\infty(\hat{x};\,\Omega)\\
&= T(\theta_{\hat{x}})\int_{\partial\Omega}\left\{u^s(y;\,\Omega)\frac{\partial e^{-ik_\hat{x}^t\cdot y}}{\partial\nu(y)} - e^{-ik_\hat{x}^t\cdot y}\frac{\partial u^s(y;\,\Omega)}{\partial\nu(y)}\right\}ds(y)\\
&= e^{ik_(d^t-\hat{x}^t)\cdot z}T(\theta_{\hat{x}})\int_{\partial D}\left\{u^s(y;\,D)\frac{\partial e^{-ik_\hat{x}^t\cdot y}}{\partial\nu(y)} - e^{-ik_\hat{x}^t\cdot y}\frac{\partial u^s(y;\,D)}{\partial\nu(y)}\right\}ds(y)\\
&= e^{ik_(d^t-\hat{x}^t)\cdot z}u^\infty(\hat{x};\,D).
\end{aligned}$$

The proof is complete.

2.3. Scattering from sparse scatterers

In this section, we consider the scattering from sparse scatterers. Let Ω_1 and Ω_2 be two scatterers contained in $\mathbb{R}^n\_$ with

$$L := \operatorname{dist}(\Omega_1,\,\Omega_2) \gg 1. \tag{2.12}$$

In order to ease the exposition, we assume that both Ω_1 and Ω_2 are bounded C^2 domains with connected complements. For any $\mathbf{a} \in C(\partial\Omega)$, we introduce the single- and double-layer operators S_Ω: $C(\partial\Omega) \to C(\partial\Omega)$ and K_Ω: $C(\partial\Omega) \to C(\partial\Omega)$, defined respectively by

$$(S_\Omega\mathbf{a})(x) = \int_{\partial\Omega} G(x,\,y)\mathbf{a}(y)\,ds(y), \quad (K_\Omega\mathbf{a})(x) = \int_{\partial\Omega}\frac{\partial G(x,\,y)}{\partial\nu(y)}\mathbf{a}(y)\,ds(y),\ x \in \partial\Omega. \tag{2.13}$$

Moreover, by changing the integration domain in (2.13) to $\partial\Omega_1$, we denote the resulting operators by S_1 and K_1, respectively; and by changing the integration domain to $\partial\Omega_2$, we denote the resulting operators by S_2 and K_2, respectively. We refer to [10] for related mapping properties of these operators.

Lemma 2.2. *Let Ω_1 and Ω_2 be two scatterers buried in $\mathbb{R}^n\_$ as described above. Then we have*

$$u^\infty(\hat{x};\,\Omega_1 \bigcup \Omega_2) = u^\infty(\hat{x};\,\Omega_1) + u^\infty(\hat{x};\,\Omega_2) + \mathcal{O}\left(L^{\frac{1-n}{2}}\right). \tag{2.14}$$

Proof. We first consider the case that both Ω_1 and Ω_2 are sound-soft. The scattered field $u^s(x;\,\Omega_1 \cup \Omega_2)$ can be represented in the form

$$u^s(x;\,\Omega_1\cup\Omega_2)=\int_{\partial\Omega_1}\left\{\frac{\partial G(x,\,y)}{\partial\nu(y)}-iG(x,\,y)\right\}\mathbf{a}_1(y)\,ds(y)$$
$$+\int_{\partial\Omega_2}\left\{\frac{\partial G(x,\,y)}{\partial\nu(y)}-iG(x,\,y)\right\}\mathbf{a}_2(y)\,ds(y),\quad x\in\mathbb{R}^n\backslash\overline{\Omega_1\cup\Omega_2},$$

with the two densities $\mathbf{a}_1\in C(\partial\Omega_1)$ and $\mathbf{a}_2\in C(\partial\Omega_2)$. Using the homogeneous Dirichlet boundary condition, one has that the densities $\mathbf{a}_1$ and $\mathbf{a}_2$ satisfy the following system of integral equations

$$\frac{1}{2}\mathbf{a}_1+K_1\mathbf{a}_1-iS_1\mathbf{a}_1+\mathbb{K}_2\mathbf{a}_2-i\mathbb{S}_2\mathbf{a}_2=f_1\quad\text{on}\quad\partial\Omega_1,\tag{2.15}$$

$$\frac{1}{2}\mathbf{a}_2+K_2\mathbf{a}_2-iS_2\mathbf{a}_2+\mathbb{K}_1\mathbf{a}_1-i\mathbb{S}_1\mathbf{a}_1=f_2\quad\text{on}\quad\partial\Omega_2,\tag{2.16}$$

where $f_1:=-u_0$ on $\partial\Omega_1$ and $f_2:=-u_0$ on $\partial\Omega_2$. In (2.15), $\mathbb{K}_2\mathbf{a}_2-i\mathbb{S}_2\mathbf{a}_2$ is the restriction on $\partial\Omega_1$ of the potential

$$\int_{\partial\Omega_2}\left\{\frac{\partial G(x,\,y)}{\partial\nu(y)}-iG(x,\,y)\right\}\mathbf{a}_2(y)\,ds(y),$$

whereas $\mathbb{K}_1\mathbf{a}_1-i\mathbb{S}_1\mathbf{a}_1$ is the restriction on $\partial\Omega_2$ of the potential

$$\int_{\partial\Omega_1}\left\{\frac{\partial G(x,\,y)}{\partial\nu(y)}-iG(x,\,y)\right\}\mathbf{a}_1(y)\,ds(y).$$

Since the distance $L\gg 1$, by straightforward calculations, it is verified that (see, e.g., [14])

$$|G(x,\,y)|=\mathcal{O}\left(L^{\frac{1-n}{2}}\right)\quad\text{and}\quad\left|\frac{\partial G(x,\,y)}{\nu(y)}\right|=\mathcal{O}\left(L^{\frac{1-n}{2}}\right),\quad\text{for}\ \ x\in\partial\Omega_1,\ y\in\partial\Omega_2.$$

Therefore, one has

$$\|\,\mathbb{K}_2-i\mathbb{S}_2\,\|_{\mathcal{L}(C(\partial\Omega_2),C(\partial\Omega_1))}=\sup_{\|\mathbf{a}\|_{C(\partial\Omega_2)}=1}\|(\mathbb{K}_2-i\mathbb{S}_2)\mathbf{a}\,\|_{C(\partial\Omega_1)}$$
$$=\sup_{\|\mathbf{a}\|_{C(\partial\Omega_2)}=1}\max_{x\in\partial\Omega_1}\left|\int_{\partial\Omega_2}\left\{\frac{\partial G(x,\,y)}{\partial\nu(y)}-iG(x,\,y)\right\}\mathbf{a}(y)\,ds(y)\right|=\mathcal{O}\left(L^{\frac{1-n}{2}}\right).\tag{2.17}$$

It is noted that the operator $\frac{1}{2}I+K_1-iS_1\colon C(\partial\Omega_1)\to C(\partial\Omega_1)$ is bijective and the inverse $(\frac{1}{2}I+K_1-iS_1)^{-1}$ is bounded (see e.g., [10]). Then from (2.15), using the behavior (2.17), one has

$$\mathbf{a}_1=\left(\frac{1}{2}I+K_1-iS_1\right)^{-1}\left[f_1-(\mathbb{K}_2-i\mathbb{S}_2)\mathbf{a}_2\right]=\tilde{\mathbf{a}}_1+\mathcal{O}\left(L^{\frac{1-n}{2}}\right),\tag{2.18}$$

with $\tilde{\mathbf{a}}_1=(\frac{1}{2}I+K_1-i\eta S_1)^{-1}f_1$. Similarly, one can show that

$$\mathbf{a}_2=\tilde{\mathbf{a}}_2+\mathcal{O}\left(L^{\frac{1-n}{2}}\right),\tag{2.19}$$

with $\tilde{\mathbf{a}}_2 = (\frac{1}{2}I + K_2 - i\eta S_2)^{-1} f_2$. Therefore, we have

$$\begin{aligned} u^\infty(\hat{x};\, \Omega_1 \cup \Omega_2) &= T(\theta_{\hat{x}}) \int_{\partial\Omega_1} \left\{ \frac{\partial e^{-ik\_\hat{x}^t\cdot y}}{\partial \nu(y)} - e^{-ik\_\hat{x}^t\cdot y} \right\} \mathbf{a}_1(y)\, ds(y) \\ &\quad + T(\theta_{\hat{x}}) \int_{\partial\Omega_2} \left\{ \frac{\partial e^{-ik\_\hat{x}^t\cdot y}}{\partial \nu(y)} - e^{-ik\_\hat{x}^t\cdot y} \right\} \mathbf{a}_2(y)\, ds(y) \\ &= u^\infty(\hat{x};\, \Omega_1) + u^\infty(\hat{x};\, \Omega_2) + \mathcal{O}\big(L^{\frac{1-n}{2}}\big), \end{aligned}$$

where we have used the estimates (2.18) and (2.19) and the fact that

$$u^\infty(\hat{x};\, \Omega_j) = T(\theta_{\hat{x}}) \int_{\partial\Omega_1} \left\{ \frac{\partial e^{-ik\_\hat{x}^t\cdot y}}{\partial \nu(y)} - e^{-ik\_\hat{x}^t\cdot y} \right\} \tilde{\mathbf{a}}_j(y)\, ds(y), \quad j = 1, 2.$$

Next we consider the other cases. To ease the expressions, we introduce the normal derivative operators K' and H, given by

$$\begin{aligned} \big(K'_\Omega \mathbf{a}\big)(x) &:= \int_{\partial\Omega} \frac{\partial G(x, y)}{\partial \nu(x)} \mathbf{a}(y)\, ds(y), \quad \big(H_\Omega \mathbf{a}\big)(x) \\ &:= \frac{\partial}{\partial \nu(x)} \int_{\partial\Omega} \frac{\partial G(x, y)}{\partial \nu(y)} \mathbf{a}(y)\, ds(y), \; x \in \partial\Omega. \end{aligned}$$

Moreover, by changing the integration domain $\partial\Omega$ to $\partial\Omega_i$, we denote the resulting operators by K'_j and H_j, $j = 1, 2$, respectively.

For simplicity, we consider only the Neumann boundary condition, and the impedance case can be handled in a similar manner. We make use the following ansatz for the scattered wave field,

$$\begin{aligned} u^s(x;\, \Omega_1 \cup \Omega_2) &= \int_{\partial\Omega_1} \left\{ G(x, y)\mathbf{a}_1(y) + i \frac{\partial G(x, y)}{\partial \nu(y)} \big(S_0^2 \mathbf{a}_1\big)(y) \right\} ds(y) \\ &+ \int_{\partial\Omega_2} \left\{ G(x, y)\mathbf{a}_2(y) + i \frac{\partial G(x, y)}{\partial \nu(y)} \big(S_0^2 \mathbf{a}_2\big)(y) \right\} ds(y), \quad x \in \mathbb{R}^n \backslash \overline{\Omega_1 \cup \Omega_2}, \end{aligned} \tag{2.20}$$

where the two density functions $\mathbf{a}_1 \in C(\partial\Omega_1)$ and $\mathbf{a}_2 \in C(\partial\Omega_2)$. In (2.20), by S_0 we denote the single-layer operator

$$\big(S_0 \mathbf{a}\big)(x) = \int_{\partial\Omega} G_0(x, y)\mathbf{a}(y)\, ds(y), \; x \in \partial\Omega,$$

where $\partial\Omega$ could be $\partial\Omega_1$ or $\partial\Omega_2$, and for $x \neq y$,

$$G_0(x, y) := \begin{cases} -\frac{1}{2\pi} \ln |x - y|, & n = 2 \\ \frac{1}{4\pi} \frac{1}{|x - y|}, & n = 3. \end{cases}$$

By the mapping properties of S_0 (cf [10]), we note that the density functions $S_0^2 \mathbf{a}_j$, $j = 1, 2$, of the double-layer potentials in (2.20) belong to $C^{1,\alpha}(\partial\Omega_j)$, $j = 1, 2$. By using the homogeneous Neumann boundary condition, one can show that the densities $\mathbf{a}_1$ and $\mathbf{a}_2$ satisfy the following system of integral equations

$$\frac{1}{2}\mathbf{a}_1 - K_1'\mathbf{a}_1 - iH_1S_0^2\mathbf{a}_1 - \mathbb{K}_2'\mathbf{a}_2 - i\mathbb{H}_2S_0^2\mathbf{a}_2 = -u_0 \quad \text{on} \quad \partial\Omega_1, \tag{2.21}$$

$$\frac{1}{2}\mathbf{a}_2 - K_2'\mathbf{a}_2 - iH_2S_0^2\mathbf{a}_2 - \mathbb{K}_1'\mathbf{a}_1 - i\mathbb{H}_1S_0^2\mathbf{a}_1 = -u_0 \quad \text{on} \quad \partial\Omega_2, \tag{2.22}$$

where $(\mathbb{K}_2'\mathbf{a}_2)(x) := (K_{\Omega_2}'\mathbf{a}_2)(x)$ for $x \in \partial\Omega_1$, and $\mathbb{K}_1'$, $\mathbb{H}_1$, $\mathbb{H}_2$ can be defined similarly. Here, we would like to remark that the operators H_1 and H_2 are hypersingular. Nevertheless, by using the facts that $S_0^2\mathbf{a}_j \in C^{1,\alpha}(\partial\Omega_j)$ and the operators H_j are bounded from $C^{1,\alpha}(\partial\Omega_j)$ into $C^{0,\alpha}(\partial\Omega_j)$, $j = 1, 2$ (cf [10]), we conclude that the composite operators $H_iS_0^2$: $C(\partial\Omega_i) \to C(\partial\Omega_j)$, $j = 1, 2$, are compact. Finally, by using a completely similar argument to the sound-soft case, one can deduce (2.14) for the Neumann boundary value problem.

The proof is complete.

We would like to remark that by using the mapping properties of the single- and double-layer boundary integral operators in [23], one can show that similar results to lemma 2.2 hold when Ω_1 and Ω_2 are Lipschitz domains.

2.4. Scattering from multiple small scatterers

Hereonin, we assume that the wave number $k = \mathcal{O}(1)$. Hence, the size of a scatterer Ω can be characterized by its Euclidean diameter. Let $D_j \subset \mathbb{R}^n_-$, $j = 1, 2, \ldots, l$ be a family of base scatterers. For technical reasons, we assume that ∂D_j, $j = 1, 2, \ldots, l$ are C^2 continuous in this section. Let $\rho \in \mathbb{R}_+$ with $\rho \ll 1$, and

$$\Omega_j^p = \left(D_j^p; z_j, \rho\right) := z_j + \rho D_j^p, \quad j = 1, 2, \ldots, l, \tag{2.23}$$

where $z_j \in \mathbb{R}^n_-$ and $p = s$, h or i, representing the type of the scatterer. It is assumed that $\Omega_j^p \subset \mathbb{R}^n_-$. Set

$$\Omega^p = \bigcup_{j=1}^{l} \Omega_j^p, \tag{2.24}$$

which represents the multiple small scatterers for our inverse scattering reconstruction. For the scatterer Ω^p introduced in (2.24), we further assume that

$$L := \min_{1\leqslant j,j'\leqslant l, j\neq j'} \operatorname{dist}(z_j, z_{j'}) \gg 1. \tag{2.25}$$

This means, the obstacle components of Ω^p in (2.24) are sparsely distributed.

Let $Y_\alpha^\beta(\cdot)$ for $\alpha \in \mathbb{N} \cup \{0\}$ and $\beta = -\alpha, \ldots, \alpha$ be the spherical harmonics which form a complete orthonormal system in $L^2(\mathbb{S}^{n-1})$ (cf [10]). In particular, we recall the spherical harmonics $Y_\alpha^\beta(\hat{x})$ of order $\alpha = 0, 1$, for $\hat{x} = (\hat{x}^l)_{l=1}^n \in \mathbb{S}^{n-1}$. In the three-dimensional case,

$$Y_0^0(\hat{x}) = \sqrt{\frac{1}{4\pi}}, \quad Y_1^{-1}(\hat{x}) = \sqrt{\frac{3}{8\pi}}\left(\hat{x}^1 - i\hat{x}^2\right),$$

$$Y_1^0(\hat{x}) = \sqrt{\frac{3}{4\pi}}\hat{x}^3, \quad Y_1^1(\hat{x}) = \sqrt{\frac{3}{8\pi}}\left(\hat{x}^1 + i\hat{x}^2\right).$$

In the two-dimensional case, Y_1^0 does not exist and

$$Y_0^0(\hat{x}) = \sqrt{\frac{1}{2\pi}}, \quad Y_1^{-1}(\hat{x}) = \sqrt{\frac{1}{2\pi}}\left(\hat{x}^1 - i\hat{x}^2\right), \quad Y_1^1(\hat{x}) = \sqrt{\frac{1}{2\pi}}\left(\hat{x}^1 + i\hat{x}^2\right).$$

We are in a position to present the main result of this section on the scattering from multiple small scatterers.

Theorem 2.1. *Let Ω^p be the multiple small scatterers as described in (2.23)–(2.25). Let $u^\infty(\hat{x};\Omega^p) \in L^2(\mathbb{S}_+^{n-1})$ be the scattering amplitude corresponding to a single incident plane wave $u^i(x) = e^{ik_+ x\cdot d^i}$. Then, for sufficiently large* L, *as $\rho \to +0$, the scattering amplitude corresponding to the sound-soft case satisfies*

$$u^\infty(\hat{x};\Omega^s) = \rho^{n-2}(\ln\rho)^{n-3}\, T(\theta_{\hat{x}})Y_0^0(\hat{x}^t)\sum_{j=1}^{l} c_j^s e^{ik_-\left(d^t-\hat{x}^t\right)\cdot z_j} + \mathcal{O}\left(\rho^{2n-4}(\ln\rho)^{2n-6} + L^{\frac{1-n}{2}}\right), \tag{2.26}$$

where c_j^s are constants depending on D_j, k_- and d^i, but independent of ρ. *In the case when $p = i$, we have*

$$u^\infty(\hat{x};\Omega^i) = \rho^{n-1}T(\theta_{\hat{x}})Y_0^0(\hat{x}^t)\sum_{j=1}^{l} c_j^e \overline{\lambda_j} e^{ik_-\left(d^t-\hat{x}^t\right)\cdot z_j} + \mathcal{O}\left(\rho^n(\ln\rho)^{3-n} + L^{\frac{1-n}{2}}\right), \tag{2.27}$$

where $\hat{\lambda}_j := \int_{\partial\Omega_j} \lambda_j ds \Big/ |\partial\Omega_j|$ and c_j^e are constants depending on D_j, k_- and d^i, *but independent of* ρ. *In the case when $p = h$, the scattering amplitude satisfies*

$$u^\infty(\hat{x};\Omega^h) = \rho^n T(\theta_{\hat{x}})\sum_{j=1}^{l}\sum_{\alpha=0}^{1}\sum_{\beta=-\alpha}^{\alpha} c_{\alpha,\beta,j}^h e^{ik_-\left(d^t-\hat{x}^t\right)\cdot z_j} Y_\alpha^\beta(\hat{x}^t) + \mathcal{O}\left(\rho^{n+1}(\ln\rho)^{3-n} + L^{\frac{1-n}{2}}\right), \tag{2.28}$$

where $c_{\alpha,\beta,j}^h$ are constants depending on D_j, k_- and d^i, but independent of ρ, *and Y_1^0 should be removed from the summation in (2.28) for the two-dimensional case.*

Proof. By lemma 2.2, it is sufficient to prove the case with a single scatterer of the form $\Omega = z + \rho D$. We shall present the proof mainly for the sound-soft case, namely (2.26), and mention the major modifications required for the sound-hard and impedance cases, namely (2.27) and (2.28), after the proof of lemma 2.3.

We first derive the asymptotic expansion of the Green function $G(x, y)$ introduced in section 2.1 as $|x - y| \to +0$. Using the series expansions of the Hankel functions and the exponential function we find that for $|x - y| \to +0$,

$$G(x,y) = G_0(x,y) + G^r(x,y) + \begin{cases} \frac{ik_-}{4\pi} + \mathcal{O}(|x-y|), & n = 3; \\ \frac{i}{4} - \frac{1}{2\pi}\ln\frac{k_-}{2} - \frac{C_E}{2} + \mathcal{O}\left(|x-y|^2\ln|x-y|\right), & n = 2, \end{cases} \tag{2.29}$$

and

$$\nabla_y G(x, y) = \nabla_y G_0(x, y) + \nabla_y G^r(x, y) + \begin{cases} \mathcal{O}\big(|x-y|^2\big), & n = 3; \\ \frac{-k^2}{4\pi}(x-y)\ln(|x-y|) + \mathcal{O}(|x-y|), & n = 2, \end{cases} \tag{2.30}$$

where $C_E := \lim_{p\to\infty}\left\{\Sigma_{m=1}^{p}\frac{1}{m} - \ln p\right\} \approx 0.57721566$ denotes Euler's constant and

$$G_0(x, y) := \frac{1}{4\pi|x-y|},\ n = 3; \quad \frac{1}{2\pi}\ln\frac{1}{|x-y|},\ n = 2,$$

represents the fundamental solution of the Laplace equation. In the above derivation, we have used the fact that $G^r(\,\cdot\,, y)$ is an analytic function in $\mathbb{R}^n_{\pm}$.

Next, for any $\mathbf{a} \in C(\partial B)$, $(B = D, \Omega)$, we introduce the boundary integral operators S_B: $C(\partial B) \to C(\partial B)$, K_B: $C(\partial B) \to C(\partial B)$ and K_B': $C(\partial B) \to C(\partial B)$ defined by

$$\begin{aligned} \big(S_B\mathbf{a}\big)(x) &= \int_{\partial B} \mathbf{a}(y) G(x, y)\, ds(y), \qquad x \in \partial B, \\ \big(K_B\mathbf{a}\big)(x) &= \int_{\partial B} \mathbf{a}(y) \frac{\partial G(x, y)}{\partial \nu(y)}\, ds(y), \quad x \in \partial B, \\ \big(K_B'\mathbf{a}\big)(x) &= \int_{\partial B} \mathbf{a}(y) \frac{\partial G(x, y)}{\partial \nu(x)}\, ds(y), \quad x \in \partial B, \end{aligned} \tag{2.31}$$

respectively. Similarly, we let S_B^0, K_B^0 and $K_B^{0,'}$ be the corresponding operators introduced in (2.31) when the integral kernel $G(x, y)$ is replaced by $G_0(x, y)$. Finally, we define M_B^0: $C(\partial B) \to C(\partial B)$ by

$$\big(M_B^0\mathbf{a}\big)(x) = \int_{\partial B} \mathbf{a}(y)\, ds(y), \quad x \in \partial B.$$

In the following, for any $x \in \partial\Omega$ we define the one-to-one corresponding point $\xi_x \in \partial D$ by $\xi_x := (x - z)/\rho$. Accordingly, for any $\mathbf{a}_D \in C(\partial D)$, we define $\mathbf{a}_\Omega \in C(\partial\Omega)$ as

$$\mathbf{a}_\Omega(x) := \mathbf{a}_D\big(\xi_x\big), \quad x \in \partial\Omega. \tag{2.32}$$

With the above preparations, we let $u^s(x; \Omega^s)$ denote the scattered wave field corresponding to Ω^s, and make use of the following ansatz

$$u^s\big(x; \Omega^s\big) = \int_{\partial\Omega}\left\{\frac{\partial G(x, y)}{\partial \nu(y)} - i\varrho G(x, y)\right\}\mathbf{a}_\Omega(y)\, ds(y), \quad x \in \mathbb{R}^n\backslash\overline{\Omega}, \tag{2.33}$$

where the coupling parameter ϱ is chosen to be

$$\varrho := \rho^{-1}(\ln\rho)^{n-3}. \tag{2.34}$$

By using the homogeneous Dirichlet boundary condition and the jumping properties of the integral operators, we see that $\mathbf{a}_\Omega \in C(\partial\Omega)$ satisfies

$$\left(\frac{1}{2}I + K_\Omega - i\varrho S_\Omega\right)\mathbf{a}_\Omega = -u^t \quad \text{on} \quad \partial\Omega, \tag{2.35}$$

where I denotes the identity operator. It is noted that the operator $\frac{1}{2}I + K_\Omega - i\varrho S_\Omega$: $C(\partial\Omega) \to C(\partial\Omega)$ is bijective (cf [10]). Hence we have for $x \in \mathbb{R}^n\backslash\overline{\Omega}$

$$u^s(x;\,\Omega^s) = -\int_{\partial\Omega}\left(\frac{\partial G(x,\,y)}{\partial\nu(y)} - i\varrho G(x,\,y)\right)\left[\left(\frac{1}{2}I + K_\Omega - i\varrho S_\Omega\right)^{-1}u^t\right](y)\,ds(y),$$

and this further implies by using (2.5) that the corresponding scattering amplitude $u_\rho^\infty(\hat{x},\,d^i)$ for $\hat{x}\in\mathbb{S}_+^{n-1}$ is given by

$$\begin{aligned}
&u^\infty(\hat{x};\,\Omega^s)\\
&= -T(\theta_{\hat{x}})\int_{\partial\Omega}\left(\frac{\partial e^{-ik_\hat{x}^t\cdot y}}{\partial\nu(y)} - i\varrho e^{-ik_\hat{x}^t\cdot y}\right)\left[\left(\frac{1}{2}I + K_\Omega - i\varrho S_\Omega\right)^{-1}u^t(\,\cdot\,,\,d^i)\right](y)\,ds(y)\\
&= iT(\theta_{\hat{x}})\int_{\partial\Omega}\left(k_\hat{x}^t\cdot\nu(y) + \varrho\right)e^{-ik_\hat{x}^t\cdot y}\left[\left(\frac{1}{2}I + K_\Omega - i\varrho S_\Omega\right)^{-1}u^t(\,\cdot\,,\,d^i)\right](y)\,ds(y).
\end{aligned}\tag{2.36}$$

Next, we introduce an operator $A_D\colon C(\partial D)\to C(\partial D)$ by

$$A_D := \frac{1}{2}I + K_D^0 - iS_D^0,\ \ n=3;\quad \frac{1}{2}I + K_D^0 + iM_D^0,\ \ n=2.\tag{2.37}$$

Then by applying lemma 2.3 in what follows and theorem 10.1 in [18] to (2.36), we have by direct calculations that

$$\begin{aligned}
&u^\infty(\hat{x};\,\Omega^s)\\
&= iT(\theta_{\hat{x}})\int_{\partial\Omega}\left(k_\hat{x}^t\cdot\nu(y) + \varrho\right)e^{-ik_\hat{x}^t\cdot y}\left[\left(\frac{1}{2}I + K_\Omega - i\varrho S_\Omega\right)^{-1}u^t(\,\cdot\,,\,d^i)\right](y)\,ds(y)\\
&= iT(\theta_{\hat{x}})\int_{\partial D}\left(k_\hat{x}^t\cdot\nu(\xi_y) + \varrho\right)\left[e^{-ik_\hat{x}^t\cdot z} + \mathcal{O}(\rho)\right]\\
&\qquad\left\{A_D^{-1}\left[u^t(z,\,d^i) + \mathcal{O}(\rho)\right] + \mathcal{O}\left(\rho^{n-2}(\ln\rho)^{n-3}\right)\right\}\rho^{n-1}\,ds(\xi_y),
\end{aligned}$$

which readily implies (2.26).

The proof is complete.

The following lemma was required in the proof of theorem 2.1.

Lemma 2.3. *Let $\Omega = z + \rho D$ and let A_D be defined in (2.37). For $\mathbf{a}_D\in C(\partial D)$, we let $\mathbf{a}_\Omega\in C(\partial\Omega)$ be defined as in (2.32). Let ϱ be given in (2.34). Then there holds*

$$\left(\frac{1}{2}I + K_\Omega - i\varrho S_\Omega\right)\mathbf{a}_\Omega = A_D\mathbf{a}_D + \mathcal{O}\left(\rho^{n-2}(\ln\rho)^{n-3}\right)\tag{2.38}$$

uniformly on $\partial\Omega$.

Proof. Using change of variables in the integrals, we have by direct computations that

$$\begin{aligned}
\left(S_\Omega^0\mathbf{a}_\Omega\right)(x) &= \int_{\partial\Omega}G_0(x,\,y)\mathbf{a}_\Omega(y)ds(y)\\
&= \frac{1}{4\pi}\int_{\partial\Omega}\frac{1}{|x-y|}\mathbf{a}_\Omega(y)\,ds(y),\ \ n=3;\\
&\quad -\frac{1}{2\pi}\int_{\partial\Omega}\ln(|x-y|)\mathbf{a}_\Omega(y)\,ds(y),\ \ n=2
\end{aligned}$$

$$= \frac{1}{4\pi}\int_{\partial D}\frac{1}{\rho\left|\xi_x-\xi_y\right|}\mathbf{a}_D\left(\xi_y\right)\rho^2\, ds\left(\xi_y\right),\ \ n\ \ 3;$$
$$-\frac{1}{2\pi}\int_{\partial} D\,\ln\left(\rho\left|\xi_x-\xi_y\right|\right)\mathbf{a}_\Omega(y)\rho\, ds\left(\xi_y\right),\ n=2$$
$$= \rho\left(S_D^0\mathbf{a}_D\right)\left(\xi_x\right),\ \ n=3;\ -\rho\ln\rho\left(M_D^0\mathbf{a}_D\right)\left(\xi_x\right)+O(\rho),\ \ n=2. \tag{2.39}$$

and

$$\left(K_\Omega^0\mathbf{a}_\Omega\right)(x)=\int_{\partial\Omega}\frac{\partial G_0(x,y)}{\partial\nu(y)}\mathbf{a}_\Omega(y)\, ds(y)=\frac{1}{2^{n-1}\pi}\int_{\partial\Omega}\frac{\nu(y)\cdot(x-y)}{|x-y|^n}\mathbf{a}_\Omega(y)\, ds(y)$$
$$=\frac{1}{2^{n-1}\pi}\int_{\partial D}\frac{\nu\left(\xi_y\right)\cdot\left(\xi_x-\xi_y\right)}{\rho^{n-1}\left|\xi_x-\xi_y\right|^n}\phi_\Omega\left(\xi_y\right)\rho^{n-1}\, ds\left(\xi_y\right)=\left(K_D^0\mathbf{a}_D\right)\left(\xi_x\right). \tag{2.40}$$

Since $G^r(\,\cdot\,,y)$ is an analytic function in $\mathbb{R}^n_-$, we see

$$G^r(x,y)=\mathcal{O}(1)\quad\text{and}\quad|\nabla_y G^r(x,y)|=\mathcal{O}(1)\qquad\text{as } |x-y|\to+0$$

and hence by (2.29) and (2.30) we can show that

$$G(x,y)-G_0(x,y)=\mathcal{O}(1)\quad\text{and}\quad|\nabla_y\left[G(x,y)-G_0(x,y)\right]|=\mathcal{O}(1)\qquad\text{as } |x-y|\to 0.$$

This further implies that as $\rho\to+0$

$$\left(\left(S_\Omega-S_\Omega^0\right)\mathbf{a}_\Omega\right)(x)=\int_{\partial\Omega}\left[G(x,y)-G_0(x,y)\right]\mathbf{a}_\Omega(y)ds(y)$$
$$=\int_{\partial D}\mathcal{O}(1)\mathbf{a}_D\left(\xi_y\right)\rho^{n-1}\, ds\left(\xi_y\right)=\mathcal{O}\left(\rho^{n-1}\right), \tag{2.41}$$

and

$$\left(\left(K_\Omega-K_\Omega^0\right)\mathbf{a}_\Omega\right)(x)=\int_{\partial\Omega}\left(\frac{\partial\left[G(x,y)-G_0(x,y)\right]}{\nu(y)}\right)\mathbf{a}_\Omega(y)\, ds(y)$$
$$=\int_{\partial D}\mathcal{O}(1)\mathbf{a}_D\left(\xi_y\right)\rho^{n-1}\, ds\left(\xi_y\right)=\mathcal{O}\left(\rho^{n-1}\right). \tag{2.42}$$

Finally, by combining (2.39)–(2.42), we readily have (2.38).

The proof is complete.

In the rest of this section, we give the necessary modifications required for proving theorem 2.1 in the sound-hard and impedance cases, namely (2.27) and (2.28). In doing so, we take the Neumann boundary condition in (1.9) a special impedance boundary condition with $\lambda\equiv 0$ on $\partial\Omega$. We shall make use of the following asantz for the scattered wave field

$$u^s\left(x;\Omega^i\right)=\int_{\partial\Omega}G(x,y)\mathbf{a}_\Omega(y)ds(y),\quad x\in\mathbb{R}^n\backslash\overline{\Omega}, \tag{2.43}$$

where $\mathbf{a}_\Omega\in C(\partial\Omega)$ can be shown to satisfy the following integral equation

$$\left(-\frac{1}{2}I+K_\Omega'+i\lambda S_\Omega\right)\mathbf{a}_\Omega=-f_\Omega:=-\frac{\partial u^t}{\partial\nu}-i\lambda u^t\quad\text{on }\partial\Omega. \tag{2.44}$$

Similar to the sound-soft case, we define $f_D\in C(\partial D)$ by $f_D(\xi_x):=f_\Omega(x)$ for all $\xi_x\in\partial D$. The operator $-\frac{1}{2}I+K_\Omega'+i\lambda S_\Omega\colon C(\partial\Omega)\to C(\partial\Omega)$ is bijective and the inverse

$(-\frac{1}{2}I + K_\Omega' + i\lambda S_\Omega)^{-1}: C(\partial\Omega) \to C(\partial\Omega)$ is bounded provided that k_-^2 is not a Dirichlet eigenvalue of $-\Delta$ in Ω. Such an assumption on k_-^2 can always be fulfilled by noting that we are only interested in the asymptotic behavior of u_ρ^s as $\rho \to +0$, and hence we may choose that $\rho < \pi/(2k_-)$ which ensures that k_-^2 is not a Dirichlet eigenvalue of $-\Delta$ in Ω (see section 5.1 in [10]). The next lemma is an important ingredient and is a counterpart to lemma 2.3, whose proof follows from a similar argument to that of lemma 2.3.

Lemma 2.4. *For $\mathbf{a}_D \in C(\partial D)$, we let $\mathbf{a}_\Omega \in C(\partial\Omega)$ be defined as in (2.32). Then there holds*

$$\begin{aligned}&\left(-\frac{1}{2}I + K_\Omega' + i\lambda S_\Omega\right)\mathbf{a}_\Omega\\ &= \left(-\frac{1}{2}I + K_D^{0,\prime}\right)\mathbf{a}_D + \mathcal{O}\left(\rho^{2-\tau_\lambda}(\ln\rho)^{3-n}\right)\end{aligned} \tag{2.45}$$

uniformly on $\partial\Omega$. In (2.45), $\tau_\lambda := 0$ if $\lambda \equiv 0$, otherwise $\tau_\lambda := 1$.

The operator $-\frac{1}{2}I + K_D^{0,\prime}: C(\partial D) \to C(\partial D)$ is bijective and its inverse is bounded (see theorem 6.26 in [18]). Using theorem 10.1 in [18], lemma 2.4 implies that for any $\mathbf{a}_D \in C(\partial D)$,

$$\begin{aligned}&\left(-\frac{1}{2}I + K_\Omega' + i\lambda S_\Omega\right)^{-1}\mathbf{a}_\Omega\\ &= \left(-\frac{1}{2}I + K_D^{0,\prime}\right)^{-1}\mathbf{a}_D + \mathcal{O}\left(\rho^{2-\tau_\lambda}(\ln\rho)^{3-n}\right).\end{aligned} \tag{2.46}$$

By (2.43)–(2.46), the scattering amplitude of the scattered field u_ρ^s on $\mathbb{S}_+^{n-1}$ is given by

$$\begin{aligned}u^\infty(\hat{x};\Omega^i) &= -T(\theta_{\hat{x}})\int_{\partial\Omega} e^{-ik_-\hat{x}^t\cdot y}\left[\left(-\frac{1}{2}I + K_\Omega' + i\lambda S_\Omega\right)^{-1} f_\Omega\right](y)\,ds(y)\\ &= -T(\theta_{\hat{x}})\int_{\partial D} e^{-ik_-\hat{x}^t\cdot y}\left[\left(-\frac{1}{2}I + K_D^{0,\prime}\right)^{-1} f_D\right.\\ &\quad \left. + \mathcal{O}\left(\rho^{2-\tau_\lambda}(\ln\rho)^{3-n}\right)\right](\xi_y)\rho^{n-1}\,ds(\xi_y).\end{aligned} \tag{2.47}$$

Using the series expansion, one has

$$\begin{aligned}e^{-ik_-\hat{x}^t\cdot y} &= e^{-ik_-\hat{x}^t\cdot(z+\rho\xi_y)} = e^{-ik_-\hat{x}^t\cdot z}\left[1 - \rho ik_-\hat{x}^t\cdot\xi_y + \mathcal{O}(\rho^2)\right],\\ u^t(y) &= T(\theta)e^{ik_-(z+\rho\xi_y)\cdot d^t} = T(\theta)e^{ik_-z\cdot d^t}[1 + \mathcal{O}(\rho)],\end{aligned}$$

and

$$\frac{\partial u^t}{\partial\nu}(y) = T(\theta)ik_-\left(\nu(\xi_y)\cdot d^t\right)e^{ik_-z\cdot d^t}\left[1 + \rho ik_-(\xi_y\cdot d^t) + \mathcal{O}(\rho^2)\right]$$

as $\rho \to +0$. Inserting these asymptotic estimates into (2.47), we finally have by straightforward calculations that

$$\begin{aligned}u_\rho^\infty(\hat{x};\Omega^i) &= \rho^{n-1}T(\theta_{\hat{x}})e^{ik_-z\cdot(d^t-\hat{x}^t)}\hat{\lambda}c_1 + \rho^n T(\theta_{\hat{x}})e^{ik_-z\cdot(d^t-\hat{x}^t)}(c_2 + \hat{x}^t\cdot C_3)\\ &\quad + \mathcal{O}\left(\rho^{n+1-\tau_\lambda}(\ln\rho)^{3-n}\right),\end{aligned} \tag{2.48}$$

where $\hat{\lambda} := \int_{\partial\Omega} \lambda(y) ds(y)/|\partial\Omega|$, c_1, c_2 are constants and C_3 is a constant vector depending on D, k_- and d^i, but independent of ρ. (2.48) readily implies (2.27) and (2.28).

3. Recovery scheme

The present section is devoted to our study on recovering multiple multiscale anomalies buried in a two-layered medium. The general structure is described as follows. First, we develop Scheme S to recover multiple small scatterers buried in a two-layered medium. Then, we develop Scheme R to recover multiple buried anomalies of regular size. Finally, using a local tuning technique to combine Schemes S and R, we obtain the final Scheme M to recover multiple multiscale buried anomalies. With the preparations in the previous section, the general strategy follows from those developed in [19–21] for recovering scatterers located in a homogeneous space. Hence, we shall focus on the necessary modifications and be sketchy at certain points by referring to [19–21] for more details.

Let Ω^p be the multiple small scatterers as described in (2.23)–(2.25). Let $u^\infty(\hat{x}; \Omega^p) \in L^2(\mathbb{S}_+^{n-1})$ be the scattering amplitude corresponding to a single incident plane wave $u^i(x) = e^{ik_+ x\cdot d^i}$. We next develop Scheme S to recover Ω^p by knowledge of $u^\infty(\hat{x}; \Omega^p)$. To that end, we introduce the following imaging functional

$$J_S^p(z) := \frac{1}{\| u^\infty(\hat{x}; \Omega^p)\|^2_{L^2(\mathbb{S}_+^{n-1})}} \sum_{\alpha=0}^{\kappa(p)} \sum_{\beta=-\alpha}^{\alpha} \left| \left\langle u^\infty(\hat{x}; \Omega^p),\, T(\theta_{\hat{x}}) e^{ik_-(d^t-\hat{x}^t)\cdot z} Y_\alpha^\beta(\hat{x}^t) \right\rangle_{L^2(\mathbb{S}_+^{n-1})} \right|^2, \tag{3.1}$$

where $\langle u, v\rangle_{L^2(\mathbb{S}_+^{n-1})} = \int_{\mathbb{S}_+^{n-1}} u \cdot \bar{v}\, ds(\hat{x})$, and $\kappa(p) = 0$ if $p = s, i$, and $\kappa(p) = 1$ if $p = h$.

It is emphasized that there is no harmonic function $Y_1^0(\hat{x})$ in the two-dimensional case, so it should be removed from the summation in (3.1) in defining $J_S^p(z)$. Clearly, $J_S^p(z)$ is a non-negative function for $z \in \mathbb{R}_-^n$.

The next theorem about the local maximum behavior of $J_S^p(z)$, $p = s, i$, is the core of our Scheme S.

Theorem 3.1. *Let Ω^p and $J_S^p(z)$ be described as in (2.24) and (3.1), respectively. Set*

$$\Theta_j^p := \frac{\| u^\infty(\hat{x}; \Omega_j^p)\|^2_{L^2(\mathbb{S}_+^{n-1})}}{\| u^\infty(\hat{x}; \Omega^p)\|^2_{L^2(\mathbb{S}_+^{n-1})}}, \quad j = 1, \ldots, l.$$

Then we have for $p = s, i$,

$$\Theta_j^p = \Theta_j^{0,p} + \mathcal{O}\left(L^{\frac{1-n}{2}} + \rho^{n-2}(\ln \rho)^{n-3}\right), \quad j = 1, \ldots, l, \tag{3.2}$$

where $\Theta_j^{0,p}$ is a positive number independent of L and ρ. Moreover, there exists an open neighborhood of z_j, $\mathrm{neigh}(z_j)$, $1 \leqslant j \leqslant l$, such that

$$J_S^p(z) \leqslant \Theta_j^{0,p} + \mathcal{O}\left(L^{\frac{1-n}{2}} + \rho^{n-2}(\ln \rho)^{n-3}\right) \quad \text{for } z \in \mathrm{neigh}(z_j), \tag{3.3}$$

where the equality holds only at $z = z_j$. That is, z_j is a local maximizer of $J_S^p(z)$ in $\mathrm{neigh}(z_j)$.

Proof. Without loss of generality, we consider only the local maximum behavior of $J_S^s(z)$ in $B_\rho(z_1)$, namely, a ball of radius ρ centered at z_1. Clearly, one has

$$|z_j - z| \geqslant L \gg 1 \quad \text{for} \quad z \in B_\rho(z_1) \quad \text{and} \quad j = 2, 3, \ldots, l. \tag{3.4}$$

Hence, by (2.14), (2.26) and (3.4), and using the Riemann–Lebesgue lemma about oscillatory integrals, one has by direct calculations that

$$J_S^s(z) = \Theta_1^s + \mathcal{O}\Big(L^{\frac{1-n}{2}}\Big) \quad \text{for} \quad z \in B_\rho(z_1). \tag{3.5}$$

Next, by (2.26), we clearly have that

$$\| u^\infty(\hat{x}; \Omega^s)\|^2_{L^2(\mathbb{S}^{n-1}_+)} = \rho^{2n-4}(\ln \rho)^{2n-6}\, \Upsilon_0 + \mathcal{O}\Big(L^{1-n} + \rho^{4n-8}(\ln \rho)^{4n-12}\Big), \tag{3.6}$$

where Υ_0 is a positive constant independent of L and ρ. Using (2.26) again, we see that for $z \in B_\rho(z_1)$

$$\begin{aligned}
&\left| \left\langle u^\infty(\hat{x}; \Omega^s),\, T(\theta_{\hat{x}}) e^{ik_-\left(d^t - \hat{x}^t\right)\cdot z} Y_0^0\left(\hat{x}^t\right) \right\rangle_{L^2\left(\mathbb{S}^{n-1}_+\right)} \right| \\
&= \rho^{n-2}(\ln \rho)^{n-3} \left| \left\langle c_1^e T(\theta_{\hat{x}}) e^{ik_-\left(d^t - \hat{x}^t\right)\cdot z_1} Y_0^0\left(\hat{x}^t\right),\, T(\theta_{\hat{x}}) e^{ik_-\left(d^t - \hat{x}^t\right)\cdot z} Y_0^0\left(\hat{x}^t\right) \right\rangle_{L^2\left(\mathbb{S}^{n-1}_+\right)} \right| \\
&\qquad + \mathcal{O}\Big(L^{\frac{1-n}{2}} + \rho^{2n-4}(\ln \rho)^{2n-6}\Big) \\
&= \rho^{n-2}(\ln \rho)^{n-3} \left| c_1^e \int_{\mathbb{S}^{n-1}_+} \left[T(\theta_{\hat{x}}) Y_0^0\left(\hat{x}^t\right) \right]^2 e^{ik_-\left(d^t - \hat{x}^t\right)\cdot (z_1 - z)}\, ds(\hat{x}) \right| \\
&\qquad + \mathcal{O}\Big(L^{\frac{1-n}{2}} + \rho^{2n-4}(\ln \rho)^{2n-6}\Big) \\
&\leqslant \rho^{n-2}(\ln \rho)^{n-3}\, |c_1^e| \int_{\mathbb{S}^{n-1}_+} \left[T(\theta_{\hat{x}}) Y_0^0\left(\hat{x}^t\right) \right]^2 ds(\hat{x}) + \mathcal{O}\Big(L^{\frac{1-n}{2}} + \rho^{2n-4}(\ln \rho)^{2n-6}\Big),
\end{aligned} \tag{3.7}$$

where the asymptotic term in the last inequality is uniformly bounded with respect to $z \in B_\rho(z_1)$ since there holds

$$\left| e^{ik_-\left(d^t - \hat{x}^t\right)\cdot (z_1 - z)} \right| \leqslant 1$$

uniformly for $z \in B_\rho(z_1)$. It is easily seen that the equality in the last estimate in (3.7) holds only at $z = z_1$. Finally, by combining (3.4)–(3.7), the proof can be completed by taking

$$\Theta_1^{0,s} = \frac{1}{\Upsilon_0} |c_1^e|^2 \left(\int_{\mathbb{S}^{n-1}_+} \left[T(\theta_{\hat{x}}) Y_0^0\left(\hat{x}^t\right) \right]^2 ds(\hat{x}) \right)^2.$$

Remark 3.1. By theorem 2.1 and (3.1), we readily see that only the leading order term of the scattered wave field $u^\infty(\hat{x}; \Omega^s)$ is used for the imaging functional $J_S^p(z)$. This means, we have linearized the nonlinear inverse scattering problem (1.1) in this case with small scatterers. In theorem 3.1, we only justified the indicating behaviors of $J_S^p(z)$ for $p = s, i$. The indicating behavior of $J_S^h(z)$ for the sound-hard case is not so evident as the sound-soft and impedance cases. Indeed, by following a completely similar argument as that for the proof of theorem 3.1, due to the integral terms involving the coupling of Y_α^β and $Y_{\alpha'}^{\beta'}$ with $\alpha \neq \alpha'$ and/or $\beta \neq \beta'$, one does not have the local maximum behavior in general. This is also evidenced by our numerical examples in what follows (see figure 6(b)), where the reconstructions of sound-hard scatterers are in general not as good as those for the sound-soft and impedance-type scatterers. This is mainly caused by the inhomogeneous background and in sharp contrast to those considered in [19, 21] with a homogeneous background space. The problematic issue can be remedied by making use of multiple far-field measurements, which shall be addressed in a forthcoming work.

Using theorem 3.1, we are now ready to formulate our first imaging scheme of locating multiple small scatterer components.

Scheme S.

1) For an unknown scatterer Ω^p in (2.24), collect the far-field data by sending a single incident plane wave $u^i(x) = e^{ikx\cdot d^i}$ with fixed k and d^i.
2) Select a sampling region in $\mathbb{R}^n_-$ with a mesh $\mathcal{T}_h$ containing Ω^p.
3) For each sampling point $z \in \mathcal{T}_h$, compute the index value $J_S(z)$.
4) Locate all the significant local maxima of $J_S(z)$ on $\mathcal{T}_h$, which represent the locations of the scatterer components.

We proceed to develop Scheme R of recovering multiple regular-size anomalies. The multiple regular-size anomalies buried in the lower half-space are first introduced as follows. Let Λ_j, $j = 1, 2, \ldots, m'$ be bounded simply connected C^2 domains in $\mathbb{R}^n_-$ that form the class of base scatterers. Set

$$\mathscr{A} := \left\{ \Lambda_j \right\}_{j=1}^{m'}. \tag{3.8}$$

In the sequel, $\mathscr{A}$ is referred to as the admissible class, and it is noted that since we do not specify the type of each base scatterer Λ_j with the superscription, it could be either sound-soft, sound-hard of impedance type. Let R_0 and R_1 be two fixed positive constants with $R_0 < R_1$, and $r_j \in [R_0, R_1]$, $j = 1, 2, \ldots, l$. Let $\Gamma_j \in \mathscr{A}$, $y_j \in \mathbb{R}^n_-$ and $U_j \in SO(n)$, $j = 1, 2, \ldots, m$ and set

$$\Sigma_j := \left(\Gamma_j;\, y_j,\, r_j,\, U_j \right), \quad j = 1, 2, \ldots, m. \tag{3.9}$$

It is assumed that $\Sigma_j \subset \mathbb{R}^n_-$. We define

$$\Sigma := \bigcup_{j=1}^{m} \Sigma_j, \tag{3.10}$$

which represents the multiple regular-size anomalies for our study. The sparsity condition is also imposed as that

$$L = \min_{1 \leqslant j, j' \leqslant m, j \neq j'} \operatorname{dist}(y_j, y_{j'}) \gg 1. \tag{3.11}$$

We emphasize again that since the type of each component obstacle of Σ is not specified with the superscription, it could be either sound-soft, sound-hard, of impedance type, or consisting of mixed-type scatterers. Scheme R developed in the following shall work to recover the scatterers in Σ. In doing so, we further require that the admissible class $\mathscr{A}$ is known in advance. Loosely speaking, the proposed Scheme R could only be used to (approximately) recover the location, scale and orientation of each scatterer component Σ_j. It is pointed out that, in the recovery process, one needs not know exactly the base scatterer Γ_j as long as it is from the admissible class $\mathscr{A}$, and its exact information will also be recovered. Moreover, we note that it is not necessary for $m' = m$. This means that certain admissible base scatterers might appear more than once or do not appear in Σ. The scenario described above covers some important applications from practice. For example, in anti-submarine detection, the possible models of the hostile submarines are known in advance which provide the admissible class $\mathscr{A}$.

We are in a position to present Scheme R. It begins with augmenting the admissible class $\mathscr{A}$ as follows. Let $\tau \in \mathbb{R}_+$ and $\tau \ll 1$. Let $\mathscr{I}_1$ be a suitably chosen finite index set, such that $\{U_j\}_{j\in\mathscr{I}_1}$ is a τ-net of $SO(n)$. That is, for any rotation matrix $U \in SO(n)$, there exists $j \in \mathscr{I}_1$ such that $\| U_j - U \| \leqslant \tau$. In a similar manner, let $\mathscr{I}_2$ be a finite index set such that $\{r_j\}_{j\in\mathscr{I}_2}$ is a τ-net of $[R_0, R_1]$. We define

$$\tilde{\mathscr{A}} = \bigcup_{j=1}^{m'} \bigcup_{j_1\in\mathscr{I}_1} \bigcup_{j_2\in\mathscr{I}_2} \left(\Lambda_j;\, r_{j_2},\, U_{j_1}\right) := \left\{\tilde{\Lambda}_j\right\}_{j=1}^{m''}. \tag{3.12}$$

The following two assumptions shall be imposed on the augmented admissible class $\widetilde{\mathscr{A}}$,

(i) $u^\infty(\hat{x};\, \tilde{\Lambda}_j) \neq u^\infty(\hat{x};\, \tilde{\Lambda}_{j'})$ for $j \neq j'$ and $1 \leqslant j, j' \leqslant m''$, $\hat{x} \in \mathbb{S}_+^{n-1}$;
(ii) $\| u^\infty(\hat{x};\, \tilde{\Lambda}_j)\|_{L^2\left(\mathbb{S}_+^{n-1}\right)} \geqslant \| u^\infty(\hat{x};\, \tilde{\Lambda}_{j'})\|_{L^2\left(\mathbb{S}_+^{n-1}\right)}$ for $j < j'$ and $1 \leqslant j, j' \leqslant m''$.

Assumption (ii) can be fulfilled by reordering if necessary. For assumption (i), we recall the following conjecture in the inverse acoustic scattering theory:

$$u^\infty\left(\hat{x};\, \Lambda\right) \neq u^\infty\left(\hat{x};\, \tilde{\Lambda}\right) \quad \text{if and only if} \quad \Lambda = \tilde{\Lambda}, \tag{3.13}$$

where Λ and $\tilde{\Lambda}$ are two obstacles. The formula (3.13) states that a single far-field measurement can uniquely determine an acoustic obstacle. There is a widespread belief that (3.13) holds true, but there is no progress in the literature. We refer to [22] for a closely related uniqueness result, and in this work we assume that (i) holds true.

For Scheme R, we introduce the following m'' imaging functionals

$$J_R^j(z) = \frac{\left| \left\langle u^\infty\left(\hat{x};\, \Sigma\right),\, e^{ik\left(d^t - \hat{x}^t\right)\cdot z} u^\infty\left(\hat{x};\, \tilde{\Lambda}_j\right) \right\rangle_{L^2\left(\mathbb{S}_+^{n-1}\right)} \right|}{\| u^\infty\left(\hat{x};\, \tilde{\Lambda}_j\right)\|^2_{L^2\left(\mathbb{S}_+^{n-1}\right)}},$$
$$\tilde{\Lambda}_j \in \tilde{\mathscr{A}},\ j = 1, 2, \ldots, m''. \tag{3.14}$$

The following theorem contains the indicating behaviors of the imaging functionals introduced above.

Theorem 3.2. *Suppose that $\tilde{\Lambda}_1 \in \tilde{\mathscr{A}}$ is of the following form*

$$\tilde{\Lambda}_1 = \left(\Lambda_{j_0};\, r_{\alpha_0},\, U_{\beta_0}\right) \quad \Lambda_{j_0} \in \mathscr{A},\ \beta_0 \in \mathscr{I}_1,\ \alpha_0 \in \mathscr{I}_2.$$

Suppose that in Σ, there exists $I_0 \subset \{1, 2, \ldots, m\}$ such that for $j \in \mathrm{I}_0$, the component $\Sigma_j = (\Gamma_j;\, y_j,\, r_j,\, U_j)$ satisfies

$$(i)\ \Gamma_j = \Lambda_{j_0}; \quad (ii)\ \| U_j - U_{\beta_0} \| \leqslant \tau; \quad (iii)\ \| r_j - r_{\alpha_0} \| \leqslant \tau; \tag{3.15}$$

whereas for $j \in \{1, 2, \ldots, m\}\backslash I_0$, at least one of the conditions in (3.15) is not fulfilled by the scatterer component Σ_j. Then for each y_j, $j = 1, 2, \ldots, m$, there exists an open neighborhood of y_j, $neigh(y_j)$, such that

(i) *if $j \in \mathrm{I}_0$, then*

$$J_R^1(z) \leqslant 1 + \mathcal{O}\left(\frac{1}{L} + \tau\right) \quad \forall\, z \in neigh(y_j). \tag{3.16}$$

Moreover, the equality holds in the above relation only when $z = y_j$. That is, y_j is a local maximum point for $J_R^1(z)$.

(*ii*) *if* $j \in \{1, 2, \ldots, m\} \backslash I_0$, *then there exists* $\epsilon_0 > 0$ *such that*

$$J_R^1(z) \leqslant 1 - \epsilon_0 + \mathcal{O}\left(\frac{1}{L} + \tau\right) \quad \forall\ z \in neigh(y_j). \tag{3.17}$$

Proof. By using the translation relation provided in lemma 2.1, the proof follows from a similar argument to that for theorem 3.1 in [21]

Based on theorem 3.2, Scheme R for successively recovering the multiple regular-size anomalous components in Σ is formulated as follows.

Scheme R.

1) For the admissible scatterer class $\mathscr{A}$ in (3.8), formulate the augmented admissible class $\tilde{\mathscr{A}}$ as that given in (3.12).
2) Collect in advance the scattering amplitudes associated with the admissible scatterer class $\tilde{\mathscr{A}}$ corresponding to a single incident plane wave $e^{ik_+ x\cdot d^j}$ with a fixed d^j. Reorder $\tilde{\mathscr{A}}$ if necessary so that assumption (ii) is satisfied, and verify assumption (i).
3) For an unknown scatterer Σ in (3.10), collect the scattering amplitude corresponding to the single incident plane wave as specified in 2).
4) Select a sampling region with a mesh $\mathcal{T}_h$ in $\mathbb{R}^n_-$ containing Σ.
5) Set $j = 1$ and $u_1^\infty(\hat{x}) = u^\infty(\hat{x}; \Sigma)$
6) If $j \neq 1$, then update $u^\infty(\hat{x}; \Sigma)$ to be $u_j^\infty(\hat{x})$.
7) For each sampling point $z \in \mathcal{T}_h$, compute the value of the imaging functional $J_R^j(z)$.
8) Locate all those significant local maxima of $J_R^j(z)$ satisfying $J_R^j(z) \approx 1$ for the scatterer components of the form $y + \tilde{\Lambda}_j$.
9) Remove all the sampling points inside those identified components $y + \tilde{\Lambda}_j$, say $j = 1, 2, \ldots, N_j$, found in 7) from $\mathcal{T}_h$. Subtract the individual scattering amplitudes associated with those already recovered components in 7) and their respective identified locations y_j from the total scattering amplitude according to the following formula,

$$u_j^\infty(\hat{x}) := u_j^\infty(\hat{x}) - \sum_{j=1}^{N_j} e^{ik_+\left(d^j - \hat{x}^t\right)\cdot y_j} u^\infty\left(\hat{x}; \tilde{\Lambda}_j\right) \tag{3.18}$$

10) If $\mathcal{T}_h = \varnothing$ or $j = m''$, then stop the reconstruction; otherwise, set $j := j + 1$, and go to 6).

Finally, we consider the recovery of multiple multiscale anomalies of the form

$$\mathbf{M} = \Omega^p \bigcup \Sigma, \tag{3.19}$$

where Ω^p is the scatterer in (2.24) and Σ is the one in (3.10). Additionally, we assume that

$$L = \operatorname{dist}\left(\Omega^p, \Sigma\right) \gg 1. \tag{3.20}$$

The corresponding recovery scheme is based on combining Schemes S and R by using a local tuning technique and shall be referred to as Scheme M. With Schemes S and R developed above, the combination can be done by following a completely similar process to that in [20, 21] and we shall skip it here.

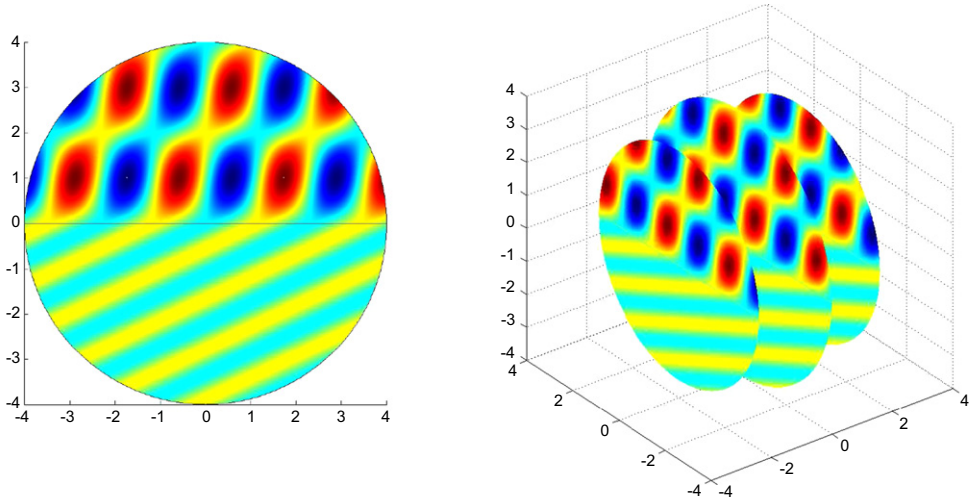

Figure 4. Plane wave scattering with no anomalies by a two-layered medium with $k_+ = \pi$ and $k_- = 2\pi$. Total wave plots in 2D (left) and in 3D (right).

4. Numerical experiments

In this section, some numerical tests are presented to demonstrate and verify the applicability of the three schemes (S, R and M) proposed for locating anomalies in a two-layered medium in both two and three dimensions. In all the tests, the exact far-field data are obtained by solving the Helmholtz system within a two-layered medium (1.2)–(1.10) using the quadratic finite elements on a truncated circular (2D) or spherical (3D) domain enclosed by a PML layer. The forward equation is solved on a sequence of successively refined meshes till the relative error of two successive finite element solutions between the two adjacent meshes is below 0.1%. Then the scattered data are transformed into the far-field data on $\mathbb{S}_+^{n-1}$ by employing the integral representation formula using (2.10) on a closed circle (2D) or surface (3D) enclosing the scatterer. For scatterers of small and regular size, we always add to the exact far-field data a uniform noise of 5% and 1%, respectively, and use them as the measurement data in our numerical tests.

It is pointed out that the ratio between k_- and k_+ is implicitly fixed due to that of the squared refractive indices in physics and has nothing to do with the inherent frequency of the detecting wave. In the sequel, we always set $k_- = 2k_+$. When there exist no anomalies, our forward solver shows the periodic structure of the transmitted wave in the lower half-space and superimposed patterns of the incident and reflected waves in the upper half-space in two and three dimensions in figure 4. In this case, the scattered wave is solely due to the two-layered medium.

Example 1: Scheme S for locating multiple small anomalies

The anomalies buried underground are multiple small sound-soft obstacles lying in the lower half-space. In the first 2D test, three little ball anomalies with radius 0.1 (in red) are laid at $(-2, -2)$, $(0, -1)$ and $(2, -1.5)$, respectively, as shown in figure 5(a).

We set the detecting wave number $k_+ = \pi$ and choose the incident direction downward with $\pi/4$ radian below the horizon $y = 0$. The detecting wave length is significantly larger

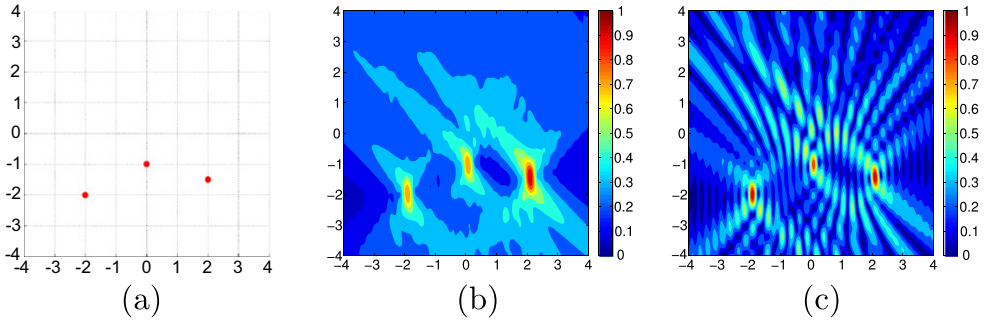

Figure 5. plane wave scattering by interface:(a) True anomalies in 2D; (b) Imaging of anomalies with ($k_+ = \pi$); (c) Imaging of anomalies with $k_+ = 5\pi$.

than the sizes of all the components. Figure 5(b) shows the indicating behavior using the indicator function (3.1) of Scheme S. The three components of the unknown scatterer are reasonably located using a single detecting plane wave field. Since refraction and reflection take place at the same time on the interface, the crucial issue is that we could only collect far-field pattern in some limited aperture, which leads to the incomplete resolution of the depth information of the scatterer in the vertical direction, which explains the slender unfocused images of the positions of those anomalies in figure 5(b). But this side effect could be overcome by increasing the frequency of the detecting wave, which will yield sharper resolution of the positions. This observation holds true for the remaining tests. By further increasing the wave number $k_+ = 5\pi$, we find that each component of the scatterer is now well captured as a local maximum highlighted as red dots as shown in figure 5(c).

In the second 3D test, the underground anomalies consist of a impedance-type sphere with impedance coefficient $\lambda = 5$ with radius 0.1 located at $(-2, 0, -1.5)$, and a sound-hard square with sidelength 0.2 located at $(2, 0, -1)$. The incident wave is pointing downward with $\pi/4$ radian within the $x - z$ plane below the horizontal ground $z = 0$.

The resulting indicator function value distribution is plotted on a pair of orthogonal slice planes $x = \pm 2$ and $y = 0$ in figure 6(b). Clearly, the positions of the respective detected components match reasonably well with the ones of the exact components. As one can see, the spherical anomaly is well located, while the position of the sound-hard square is much dimer compared with its counterpart, though both are visualized in the highlighted part (local maxima). This verifies our theoretical observations made in remark 3.1.

Example 2: Scheme R for locating multiple regular-size anomalies

We adopt two regular-size anomalies as shown in figure 7, one is a triangular plate and the other is an elliptic one, both are of thickness 0.2. These two reference anomalies have six orientations as shown in figure 8.

Now we follow Scheme R to locate all the components, one by one, by computing an indicator function for each reference object in the augmented admissible class, which tells the shapes and orientations of all potential components.

In the first stage, the reference triangular anomaly is first chosen to be located, based on the reordering of the magnitudes of the far-field patterns of all the reference scatterer components. We plot in figures 9(a)–(d) the indicator function value distribution by testing reference data associated with four different orientations in figures 8(a)–(d). It clearly indicates the right position of the triangular plate when the orientation angle is 90 degrees (see the

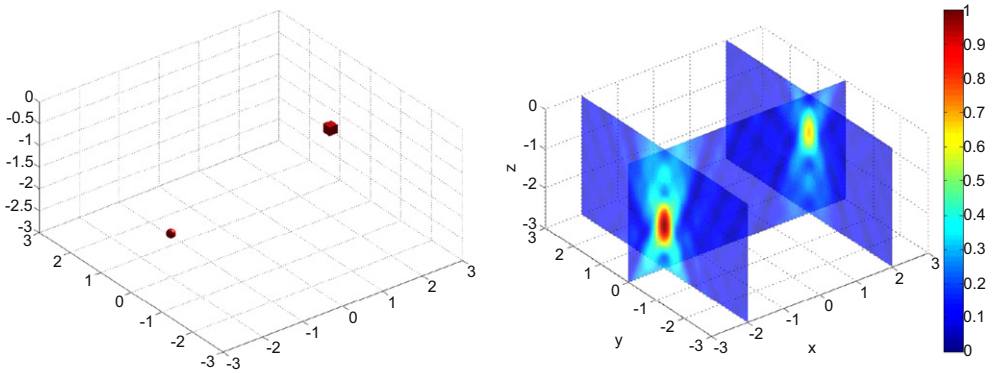

(a) (b)

Figure 6. (a) True small anomalies in 3D; (b) Imaging of anomalies by Scheme S with $(k^+ = \pi)$.

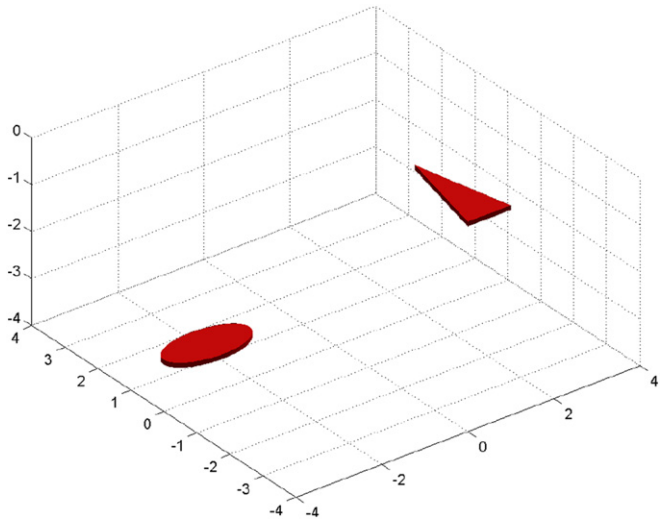

Figure 7. True regular-size anomalies: one triangular component lying at (3, 0, −2), and an elliptic component at (−3, 0, −3).

superimposed slice plots at $x = 3$ and $y = 0$ in figure 9(b)) and there is a local maximum point, which implicitly gives hints about the anomaly's shape, orientation and scale by incorporating the relevant message carried in the reference data.

Once the triangular plate anomaly is found, then we proceed by subtracting the far-field contribution of the detected triangular plate anomaly from the total far-field pattern. We can then find the elliptic plate position reasonably well by showing the superimposed slice plots at $x = -3$ and $y = 0$; see figures 8(e)–(f) and figures 9(e)–(f), respectively. We see that only the configuration with 0 degree maximizes the indicator function to achieve the maximum and indicates the position of the detected elliptic plate anomaly very clearly.

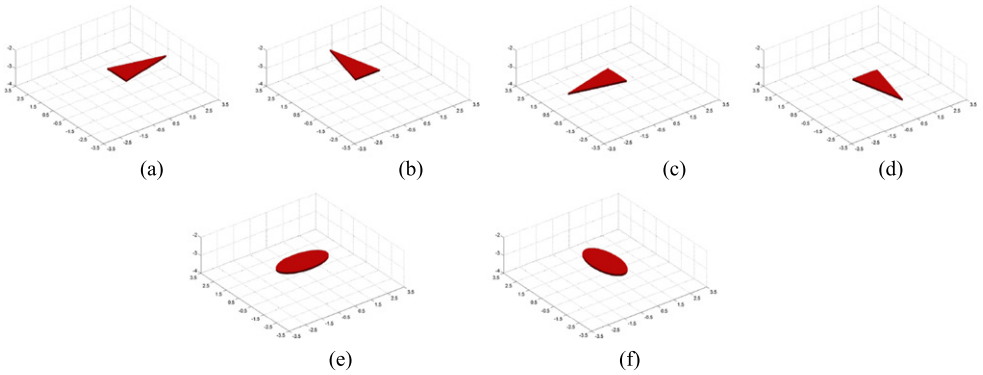

Figure 8. Reference set: (a)–(d) Triangular plate with rotation 0, 90, 180 and 270 degrees; (e)–(f) Elliptic screen with rotation 0 and 90 degrees.

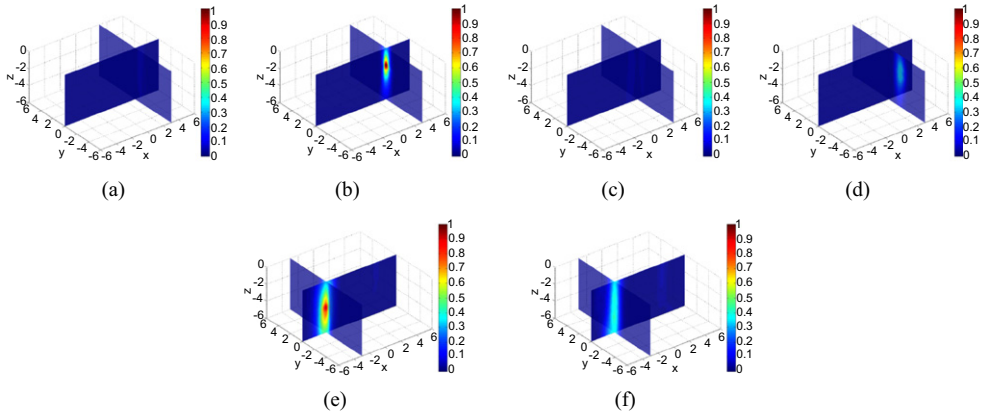

Figure 9. Results of locating two regular-sized scatterer

Example 3: Scheme M for locating multiple multiscale anomalies

We now consider a scenario of multiple 3D multiscale buried anomalies consisting of two components: a small spherical anomaly with radius 0.1 and a large triangular plate; see figure 10.

In the first stage, we extract the information of the regular-size component using the indicator function of Scheme R by computing the inner product between the collected far-field data and *a priori* known far-field patterns associated with those reference scatterer components with different orientations and sizes. We can find the approximate position of the larger triangular component of regular size when the reference scatterer is its orientation of 0 degree as shown in figure 11(a).

In the next stage, the location of the small spherical component can be obtained by performing a local tuning technique via searching grid points in some local cubic mesh around covering the local maximum in figure 11(a).

In figures 11(e)–(g), as the searching grid-points approach gradually from $(-3, 0, -2.95)$ to $(-3, 0, -3.05)$ (from left to right), the value distribution of the indicator function in Scheme S displays an interesting change of the highlighted position. In the middle plot in

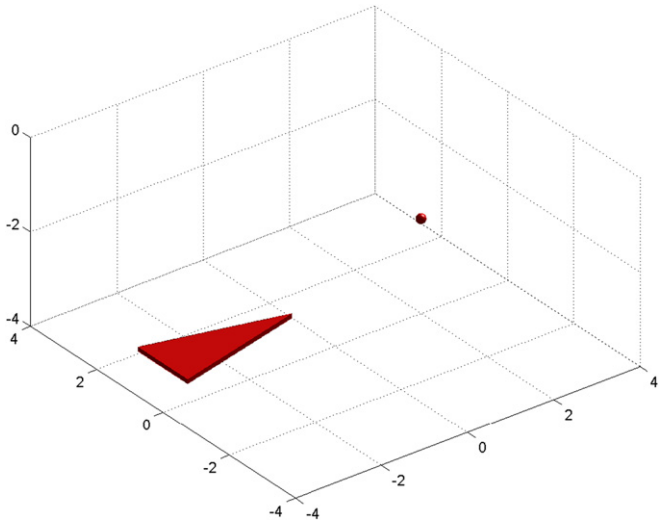

Figure 10. Underground scenario of multiple multiscale anomalies: one triangular plate anomaly lying at $(-3, 0, -3)$, and a small spherical anomaly lying at $(3, 0, -2)$.

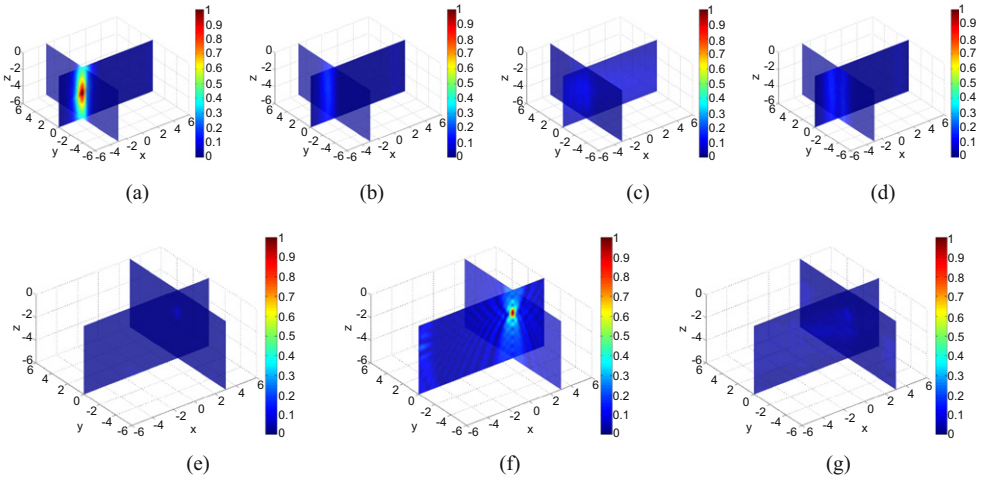

Figure 11. (a)–(d): Slice plots of the indicator function value distribution of Scheme R associated with triangular plate reference data with orientations 0, 90, 180 and 270 degrees. (e)–(g): Slice plots of the indicator function value distribution of Scheme S in the fine tuning stage by subtracting far-field data of the reference triangular plate component displaced at local mesh points $(-3, 0, -2.95)$, $(-3, 0, -3)$, and $(-3, 0, -3.05)$, respectively.

figure 11(f), the red dot indicates an approximate position of the small spherical anomaly, which agrees with the exact one $(3, 0, -3)$ very well. In such a way, the small spherical component could be positioned, and it helps us finely tune the position of the triangular component and update it to be around $(-3, 0, -3)$.

Acknowledgments

The authors would like to express their gratitudes to the two anonymous referees for their insightful and constructive comments, which have led to significant improvement on the results and presentation of this work. The work was supported by NNSF of China, No. 11201453, No. 11101412 and No. 11371115. P Li was also supported in part by the NSF grant DMS-1151308. H Liu was also supported by Hong Kong RGC General Research Fund, HKBU 12302415, and FRG grants of Hong Kong Baptist University, and the Science Research Foundation of Heilongjiang Province Educational Committee 12531139. X Liu was also supported in part by the National Center for Mathematics and Interdisciplinary Sciences, CAS.

References

[1] Ammari H, Garnier J, Jing W, Kang H, Lim M, Solna K and Wang H 2013 Mathematical and statistical methods for multistatic imaging *Lecture Notes in Mathematics* vol 2098 (Berlin: Springer)
[2] Ammari H and Kang H 2004 Reconstruction of small inhomogeneities from boundary measurements *Lecture Notes in Mathematics* vol 1846 (Berlin: Springer)
[3] Ammari H and Kang H 2007 Polarization and moment tensors. with applications to inverse problems and effective medium theory *Applied Mathematical Sciences* vol 162 (New York: Springer)
[4] Ammari H, Iakovleva E and Lesselier D 2005 A MUSIC algorithm for locating small inclusions buried in a half-space from the scattering amplitude at a fixed frequency *SIAM Multiscale Model. Simul.* **3** 597–628
[5] Bao G, Li P, Lin J and Triki F 2015 Inverse scattering problems with multifrequencies *Inverse Problems* (submitted)
[6] Bao G and Lin J 2001 Imaging of local surface displacement on an infinite ground plane: the multiple frequency case *SIAM J. Appl. Math.* **71** 1733–52
[7] Bao G, Lin J and Mefire S 2014 Numerical reconstruction of electromagnetic inclusions in three dimensions *SIAM J. Imag. Sci.* **7** 558–77
[8] Cheney M 2001 The linear sampling method and the MUSIC algorithm *Inverse Problems* **17** 591
[9] Colton D, Coyle J and Monk P 2000 Recent developments in inverse acoustic scattering theory *SIAM Rev.* **42** 369–414
[10] Colton D and Kress R 2013 *Inverse Acoustic and Electromagnetic Scattering Theory* 3rd edn (Berlin: Springer)
[11] Cutzach P M and Hazard C 1998 Existence, uniqueness and analyticity properties for electromagnetic scattering in a two-layered medium *Math. Methods Appl. Sci.* **21** 433–61
[12] Delbary F, Erhard K, Kress R, Potthast R and Schulz J 2008 Inverse electromagnetic scattering in a two-layered medium with an application to mine detection *Inverse Problems* **24** 015002
[13] Devaney A J 2000 Super-resolution processing of multi-static data using time reversal and MUSIC *Northeastern University* preprint
[14] Iakovliva E 2004 Inverse scattering from small inhomogeneities *PhD Thesis* Ecole Polytechnique
[15] Kirsch A 2002 The MUSIC-algorithm and the factorization method in inverse scattering theory for inhomogeneous media *Inverse Problems* **18** 1025
[16] Kirsch A and Grinberg N 2008 *The Factorization Method for Inverse Problems* (Oxford: Oxford University Press)
[17] Kirsch A and Liu X 2014 The factorization method for inverse acoustic scattering by a penetrable anisotropic obstacle *Math. Meth. Appl. Sci.* **37** 1159–70
[18] Kress R 2014 *Linear Integral Equations* 3rd edn (New York: Springer)
[19] Li J, Liu H, Shang Z and Sun H 2013 Two single-shot methods for locating multiple electromagnetic scatterers *SIAM J. Appl. Math.* **73** 1721–46
[20] Li J, Liu H and Wang Q 2013 Locating multiple multiscale electromagnetic scatterers by a single far-field measurement *SIAM J. Imaging Sci.* **6** 2285–309

[21] Li J, Liu H and Zou J 2014 Locating multiple multiscale acoustic scatterers *SIAM Multiscale Model. Simul.* **12** 927–52
[22] Liu X and Zhang B 2010 A uniqueness result for inverse electromagnetic scattering problem in a two-layered medium *Inverse Problems* **26** 105007
[23] Mclean W 2000 *Strongly Elliptic Systems and Boundary Integral Equations* (Cambridge: Cambridge University Press)
[24] Monk P 2003 Finite element methods for maxwell's equations *Numerical Mathematics and Scientific Computation* (New York: Oxford University Press)